NTNU – Trondheim
Norwegian University of
Science and Technology

Experimental Study of Fluid-Structure Interaction in a Simplified Geometry of the Human Upper Airways

Benjamin Broschek
Cintia Maria Golpe Sonora

Master's Thesis
Submission date: July 2015
Supervisor: Bernhard Müller, EPT
Co-supervisor: Sverre Gullikstad Johnsen, SINTEF

Norwegian University of Science and Technology
Department of Energy and Process Engineering

NTNU – Trondheim
Norwegian University of
Science and Technology

Faculty of Engineering Science and Technology
Department of Energy and Process Engineering

Master Thesis

Experimental Study of Fluid-Structure Interaction in a Simplified Geometry of the Human Upper Airways

BENJAMIN BROSCHEK
CINTIA MARIA GOLPE SOÑORA

July 2015

SUPERVISORS:
Bernhard Müller
Sverre Gullikstad Johnsen

LOCATION:
Trondheim

TIME FRAME:
July 2015

ABSTRACT

OSAS (Obstructive Sleep Apnoe Syndrome) is a sleep related breathing disorder caused by repetitive collapses of the pharyngeal walls [Figure 1] during sleep. The objective of this project is to supply experimental data to validate CFD simulations of fluid-structure Interaction (FSI), used in the prognosis of surgeries for OSAS.

A testrig to investigate the FSI of flow over a rigid plate with an attached elastic plate was designed, built and tested. Velocity profiles (derived from pitot tube pressure measurements) normal to the elastic plate and behind the elastic plate were measured as air flows by, and the motion of the elastic plate was recorded with a highspeed camera. Furthermore the recordings were analyzed and the movement of the flexible plate was determined. The experiments were realized with pitot-tube measurements and high-speed camera recordings.

We often take for granted the very things
that most deserve our gratitude.

— Cynthia Ozick

ACKNOWLEDGEMENTS

We would like to express our gratitude to our supervisor Bernhard Müller and our Co-Supervisor Sverre Gullikstad Johnsen for their help throughout the whole project, the useful comments and ideas, remarks and engagement through the learning process of this master thesis.

Furthermore we would like to thank Arnt Egil Kolstad for helping us to get all technical problems solved and for his patience, Jan Bartl for advising us with different problems during the experiments, Hennig Olav Harsvik and Pasi Alto for helping us with the CNC-machines. We also would like to express our gratitude to Lars Roar Sætran and James Dawson for their helpfulness to get all parts we needed for our experiment.Special thanks to Jon Fredrik Arnesen from Lindburg and Lund AS for for his help. Not to forget all the PhD students in the Fluids Engineering group of the Department of Energy and Process Engineering of NTNU, who willingly shared their precious time and knowledge with us.

Finally we would like to thank our families, who have supported us throughout the entire journey, by keeping us harmonious and helping us putting pieces together and never to lose the right way.

CONTENTS

LIST OF FIGURES

LIST OF TABLES

ACRONYMS

FSI	Fluid Structure Interaction
CFD	Computational Fluid Dynamics
DAQ	Data Acquisition Card
OSAS	Obstructive Sleep Apnoe Syndrome
std	Standard deviation
RANS	Reynolds Averaged Navier Stokes simulation
ALE	Arbitrary Lagrangian-Eulerian

Part I

INTRODUCTION

The first part of the project will give an little introduction to OSAS, the main research project and the range of this project.

1 OSAS

1.1 THE DISEASE

1.1.1 *Background and status of knowledge*

"OSAS is a sleep related breathing disorder caused by Nasal cavity repetitive collapses of the pharyngeal walls [Figure 1] during sleep, resulting in reduced breathing, oxygen desaturation and sleep disturbances. It is well documented that OSAS [Figure 1] has a huge impact on global health [5, 9, 11, 3]. OSAS is one of the most important contributive factors that lead to cardiovascular diseases including hypertension, stroke and ischemic heart disease." - [15]

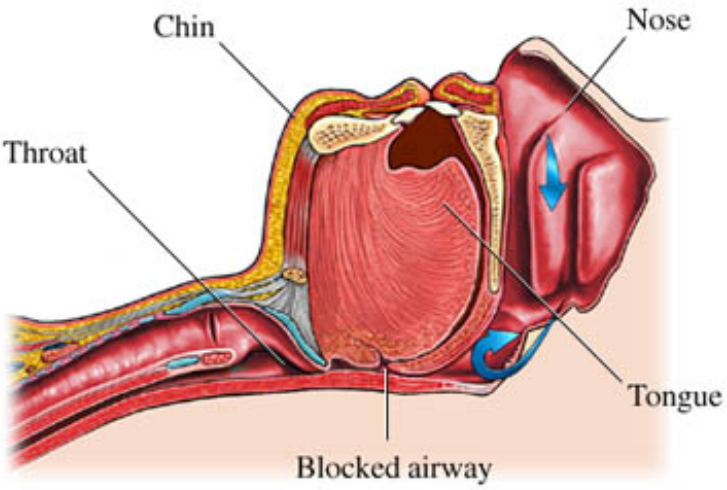

Figure 1: OSAS, [8]

"Nasal surgery, by e.g. modifying the concha or the soft palate, is relatively easy to perform and has been reported to have an effect on OSAS. However, no accepted guidelines exist on what type of nasal surgery to perform or in which subgroup of patients a positive outcome can be expected. There is a clear demand for reliable ways of predicting the success of treatment options.
To obtain realistic FSI models, measuring the mechanical properties of the soft tissue found in the pharynx is crucial. In vivo measurements are not feasible, so models can either be based on in vitro mea-

surements or on tuning of mechanical properties to match modeling results with experimental measurements. Since clinical flow measurements in the upper airways are difficult to perform on patients, flow experiments have frequently been performed on mechanical models of the human airways [13]."- [15]

1.1.2 *Treatments*

Continuous positive airway pressure (CPAP)

A common treatment for people with OSAS is the use of a continuous positive airway pressure (CPAP) device, this is a small pump continuously supplying compressed air. Normally the patients are wearing a mask that covers their nose and or mouth[Figure 2].

Figure 2: CPAP, [10]

Mandibular advancement device (MAD)

Generally used to treat mild OSAS, mandibular advancement device (MAD) [Figure 3] is a dental appliance.

Surgery

As explained in the section above surgery is not always effective and their is a risk of complications. However it gets used when

Figure 3: MAD, [4]

no other possibilities are available. Different kinds of surgeries are used.

Soft palate implants

To make the soft palate stiffer, soft pallate implants are inserted into the soft palate.[14]

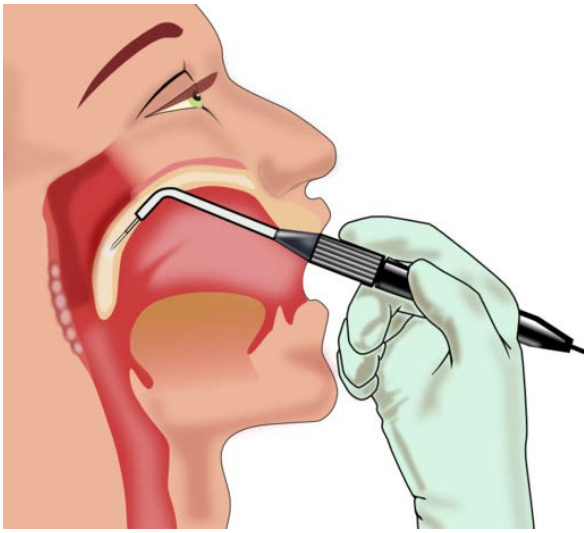

Figure 4: Soft Palate Implants, [12]

1.2 FSI

"*Fluid-structure interaction (FSI) is the interaction of some movable or deformable structure with an internal or surrounding fluid flow.[1] Fluid-structure interactions can be stable or oscillatory. In oscillatory interactions, the strain induced in the solid structure causes it to move such that the source of strain is reduced, and the structure returns to its former state only for the process to repeat.*
Fluid-structure interaction problems and multiphysics problems in general are often too complex to solve analytically and so they have to be analyzed by means of experiments or numerical simulation. Research in the fields of computational fluid dynamics and computational structural dynamics is still ongoing but the maturity of these fields enables numerical simulation of fluid-structure interaction. Two main approaches exist for the simulation of fluid-structure interaction problems:" - [1]

- Monolithic approach: the equations governing the flow and the displacement of the structure are solved simultaneously, with a single solver
- Partitioned approach: the equations governing the flow and the displacement of the structure are solved separately, with two distinct solvers

2 THE RESEARCH PROJECT

2.1 THE MAIN RESEARCH

"OSAS is caused by the failure of the muscular tissue to keep the airway open. The detailed mechanisms behind this are still unexplained, but it is clear that OSAS is caused by a complex two-way interaction between the flowing air and the soft tissue found in the upper airways. To fully appreciate the complexity of the problem it is required to employ numerical models where the air-flow is coupled to the deformations of the soft tissue. This can be done by employing Fluid Structure Interaction (FSI) modeling.
To obtain realistic FSI models, measuring the mechanical properties of the soft tissue found in the pharynx is crucial. In vivo measurements are not feasible, so models can either be based on in vitro measurements or on tuning of mechanical properties to match modeling results with experimental measurements. Since clinical flow measurements in the upper airways are difficult to perform on patients, flow experiments have frequently been performed on mechanical models of the human airways [13].
Thus, considerable challenges are associated with setting up patient specific CFD models and calibrating the FSI models. In addition, the computational costs in terms of processor-time are significant in modeling the two-way coupling between transient fluid and structural stresses in the upper airways. The current project is limited to demonstrating that this can be done by a team of experts in the relevant fields. For the extended research activity, however, in the continuation of the current project, the vision is that the current challenges can be overcome by new modeling procedures and technological advancement and that the surgeon can run patient specific simulations prior to performing surgery." - [15]

Please for more information visit the project web page [2] and the SINTEF article [16].

2.1.1 *Approaches, hypotheses and choice of method, Main Proyect*

"The proposed project lays out a challenging multidisciplinary research task that aims at bridging the gap between physiology, medical

research and technological state-of-art. To meet the multidisciplinary demands, the research team consists of specialist from St. Olavs hospital; the Faculty of Medicine (DMF), NTNU; the Faculty of Engineering Science and Technology (IVT), NTNU; and SINTEF Materials and Chemistry. The proposed project consists of four work packages:

- WP1 Clinical Research
- WP2 Soft Tissue Modeling
- WP3 Mathematical Modeling of Fluid-Structure Interaction
- WP4 CFD Modeling for Prediction of Success of OSAS Surgery

The combined effort of the work packages will result in mathematical models that can be use to predict the airflow changes in OSAS patients due to surgery to relieve nasal stenosis. The modeling results will be jointly analyzed. The medical experts will judge the model predictions by comparison with clinical facts. Thus, the potential of the developed models and the requirements of improved tools can be assessed." - [15]

2.2 OUR PART OF THE RESEARCH (WP4)

"The objective of the master project is to provide experimental support to validate a CFD benchmark model for the development of advanced fluid-structure interaction (FSI) models in the main project. The experimental work will consist of planning and building a simplified model of the human upper airways (nose, mouth, hard and soft palate, pharynx), and performing air-flow experiments in the established geometry. Experimental recordings will include, pressure and velocity field measurements as well as high-speed video recordings of the movement of the soft palate as air flows by. The experimental results will be documented to be used for the validation of CFD models of FSI. The simplified model will act as a calibration standard for models developed in both WP3 and WP4 The experimental results will be discussed with the developers of CFD models of FSI in another master project and in the main project." - [15]

Part II

DESIGN AND CONSTRUCTION

This part treats the process from the first idea to the finished testrig.

3 DESIGN

3.1 IDEAS AND RESEARCH

Based on the sketch [Figure 5] provided by our co-supervisor the design process started.

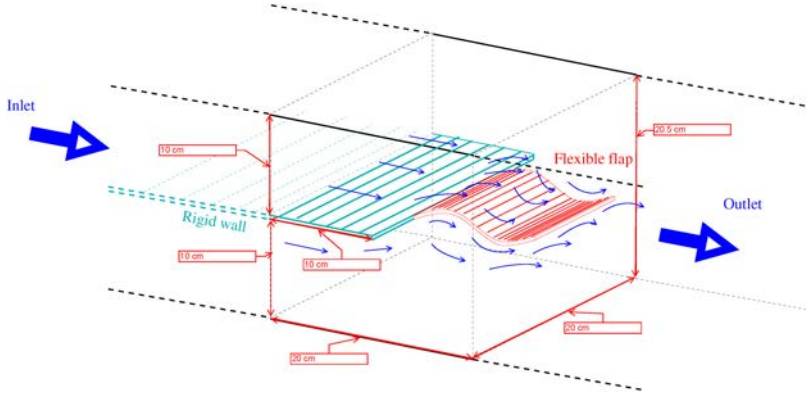

Figure 5: OSAS Experiment Sketch

The principal idea was to create a testrig in which a flexible flag interacts with an air inflow. To make this possible the flexible part was attached to a rigid part which was situated in the testrig. With this constellation an flow input should provoke an fluid-structure interaction with the flexible part producing an oscillation. The main part of the project was to measure the dynamics of the flexible part and the velocity fields.

To be able to design the "testrig" it was crucial to know which aspects of the experiments were important and which ones were secondary. In cooperation with the supervisors a list of must-have points were elaborated:

- uniform and homogeneous inflow.
- possibility to measure pressure and velocity field.
- 2-Dimensional oscillation of the flexible part

With this list in mind first layouts were drawn [Figure 6]. During the design process different suggestions and ideas, like dimension and inflow speed, helped to improve the testrig. Important aspects which have been taken in count are:

- removable and changeable flexible- and rigid part.
- possibility to extend the testrig in X-axes, to measure the field behind the flexible part.
- ability to rotate the whole construction around the Y-axis to simulate different angles.
- possibility to put the rigid- and flexible parts in horizontal and vertical position.
- adjustable input speed.
- use of material with similar properties of human tissue for the flexible part.
- the testrig needs visible access for the high-speed camera.

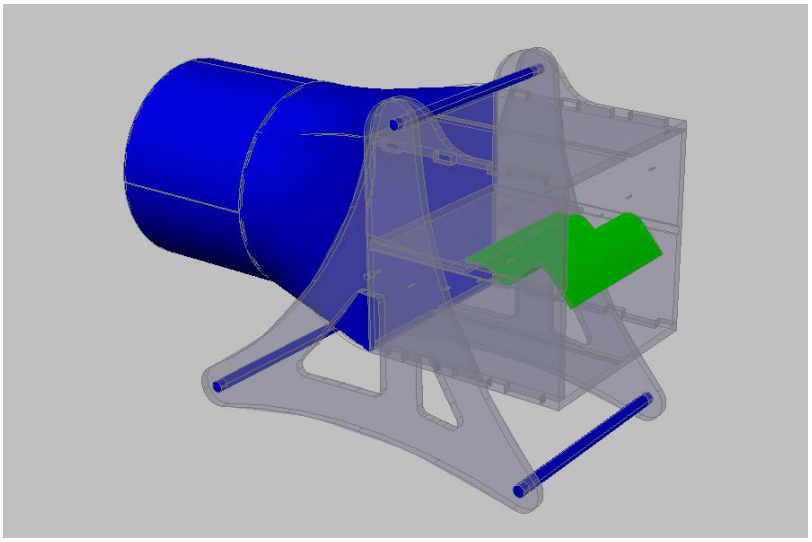

Figure 6: First Layout

After the first design we observed that the basis would be too filigree for our needs and the construction would be too time consuming. So a new design was made with a more stable and easier to build base.

3.2 FINAL DESIGN

After including all important aspects of the experiment the main design process starts. The following drawings and plans show the final design used in the experiments.

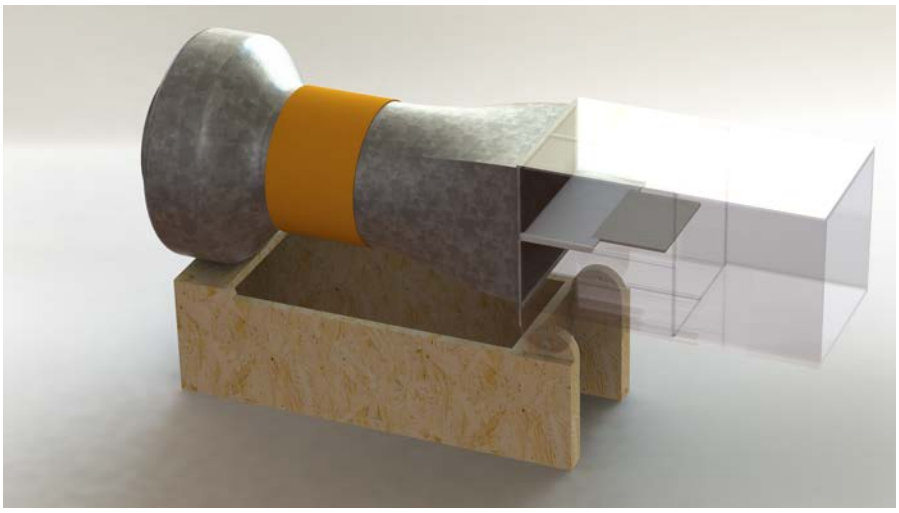

Figure 7: Final Design

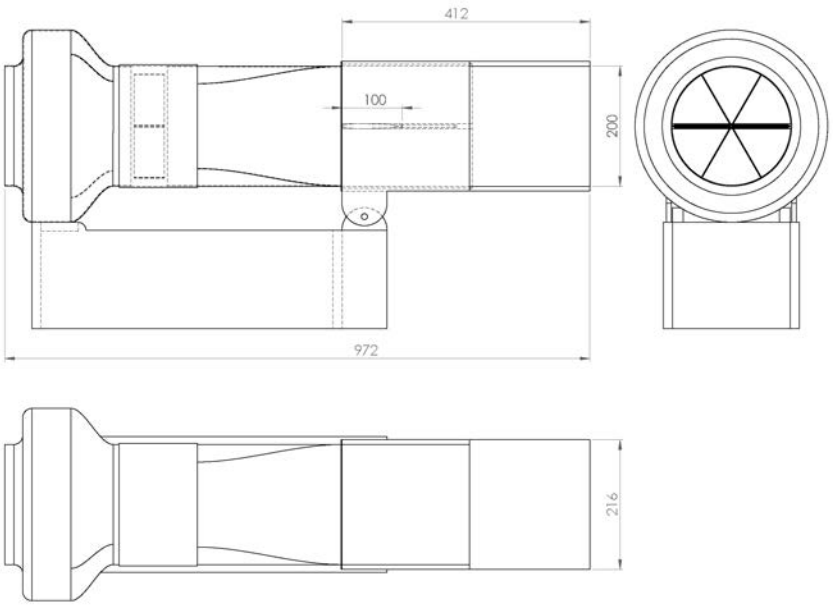

Figure 8: Overview

As shown in the figure [Figure 8], the final version consists of a stable wooden base where the cube, extension and all the

other parts are fixed. During the design process we assumed the following fluid characteristics.

$$v = 6m/s \tag{1}$$
$$\nu = 1.5 \times 10^{-5} m^2/s \tag{2}$$
$$d = 0.2m \tag{3}$$
$$Re = 80000 \tag{4}$$
$$\tag{5}$$

Detailed plans are attached in the appendix[Section A.2, Section A.3, Section A.4, Section A.5].

4

CONSTRUCTION

4.1 TESTRIG

The testrig [Figure 10] is the main part for the experiment. It is build out of the base which sustains the whole construction, the cube, in which the rigid and flexible parts are fixed and where the experiments were realized. The last part of the testrig is the fan and the conduct which connects cube and blower. The base is made out of 15mm OSB plates, the cube out of 8mm plexiglass. For the connection of fan and cube a ⌀200mm PVC tube and a 4m flexible conduct have been used. A detailed explanation and a figure [Figure 9] describing each part of the testrig are listed below:

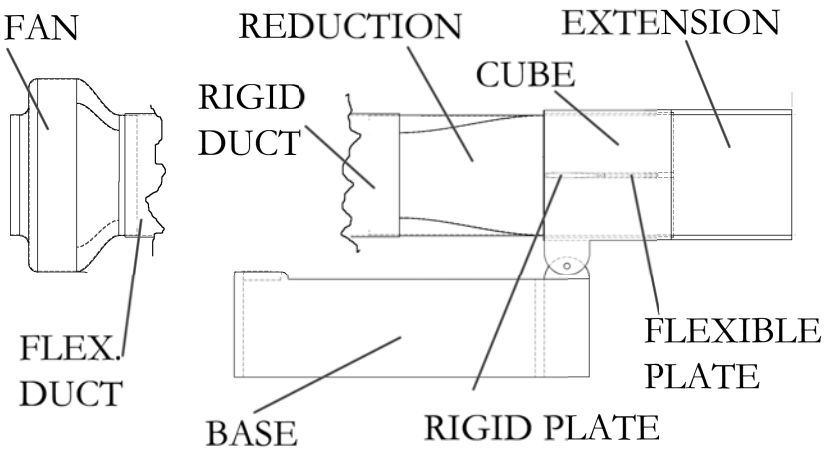

Figure 9: Overview of all parts

4.1.1 *Base*

The base, build out of 15mm OSB, and connected by standard screws, is used to maintain the whole construction. The second function is to tilt the cube about the lateral axis.

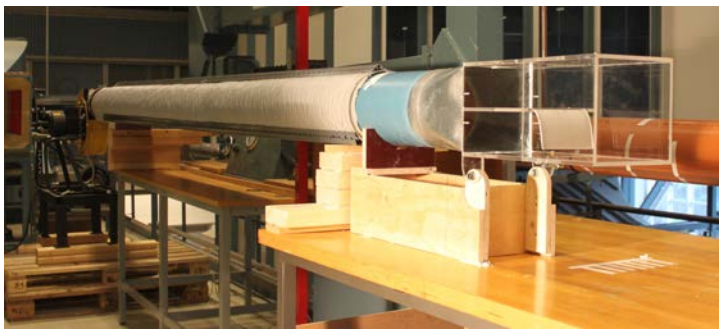

Figure 10: Finished testrig

4.1.2 *Cube*

The cube is one of the most important part [Figure 11] of the testrig, It consists of 3 individual elements:

Figure 11: Cube

- Reduction: The reduction is used as a adapter between the rectangular cube and the round conducts. It is made out of 1.5 mm galvanized sheet [Figure 11].
- Middle cube: The middle part is the main element used to fix the rigid and flexible part. Its permanently connected to the reduction on one side and has connectors for the extension on outflow side. It is made out of 8mm plexiglass[Figure 11].
- Extension: The extension has the same dimensions as the middle cube and is build out of the same material, the main function is to prolong the measurable space of the area behind the flexible part (evolution of the velocity profil)[Figure 11].

4.1.3 *Conducts*

The conducts are made out of ⌀200mm PVC tube and a ⌀200mm and 4m long flexible conduct. The flexible pipe is used to ensure a vibration free connection to the fan. The reason for using a 4m long tube was simple, it is the longest possible distance from the fan to the reduction with the space available to ensure a complete developed velocity profile. For the last meter a smooth PVC duct with honeycomb (after different tests it results that there is no need for the honeycomb) has been installed to guarantee a laminar and uniform flow. Between fan and flexible tube a mesh was inserted, to improve the flow characteristics.

4.1.4 *Blower*

1st Blower

(a) Main Part of the blower

(b) Top part of the blower

(c) First Blower

Figure 12: First Blower with improvements

From the beginning the experiment was designed to use an fan with an low input flow velocity (1-7m/s) [Figure 12,Figure 15]. For this purpose a normal radial blower with an nominal output-speed of approximately 7-9m/s was used. Due to the centripetal-effect no homogeneous flow was achieved[Figure 15]. Different corrections like guiding-blades could improve the input-flow profile[Figure 12]. Even though after first FSI tests the input-velocity was too small as to provoke real oscillations in the flexible part[Table 1].

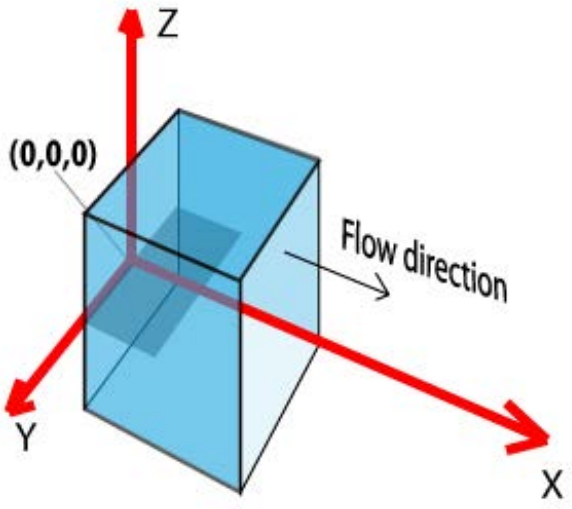

Figure 13: Coordinate-system

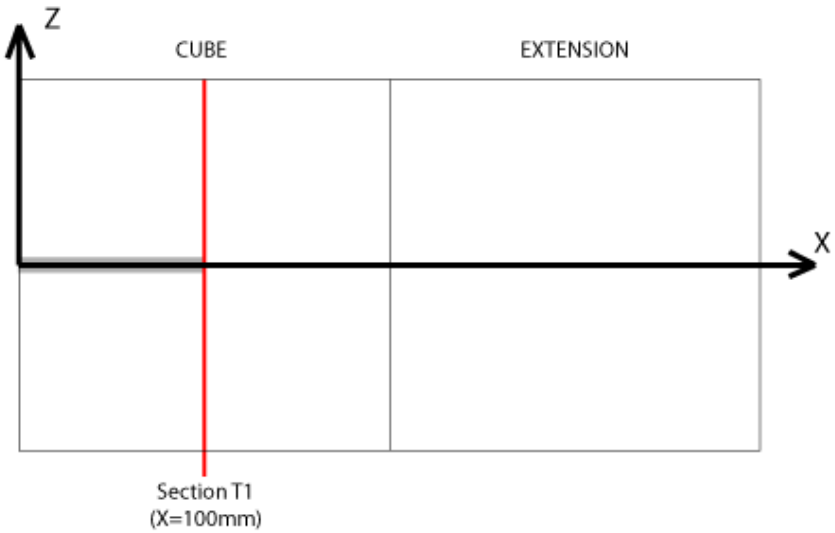

Figure 14: Section for the first Tests

To find out if a homogenous input velocity has been achieved, a first test with 9 different input-velocities were measured at 4 equal distanced points from the center of section T1 (The measurement were taken parallel to theY-axis, Z=0 and X=100mm) [Figure 13, Figure 14] horizontal over the half cross-section of the cube.

Table 1: Input flow 1st blower: $radius(m) vs velocity(m/s)$

radio(mm)	$S_1(m/s)$	$S_2(m/s)$	$S_3(m/s)$	$S_4(m/s)$	$S_5(m/s)$	$S_6(m/s)$	$S_7(m/s)$	$S_8(m/s)$	$S_9(m/s)$
0	2,74	3,10	3,30	3,65	3,86	4,30	4,60	4,90	4,98
30	2,40	2,55	2,76	3,05	3,23	3,50	3,75	4,00	4,05
60	3,50	3,80	4,25	4,66	4,95	5,40	5,75	6,05	6,30
90	3,10	3,09	3,40	3,70	4,10	4,50	4,95	5,16	5,40

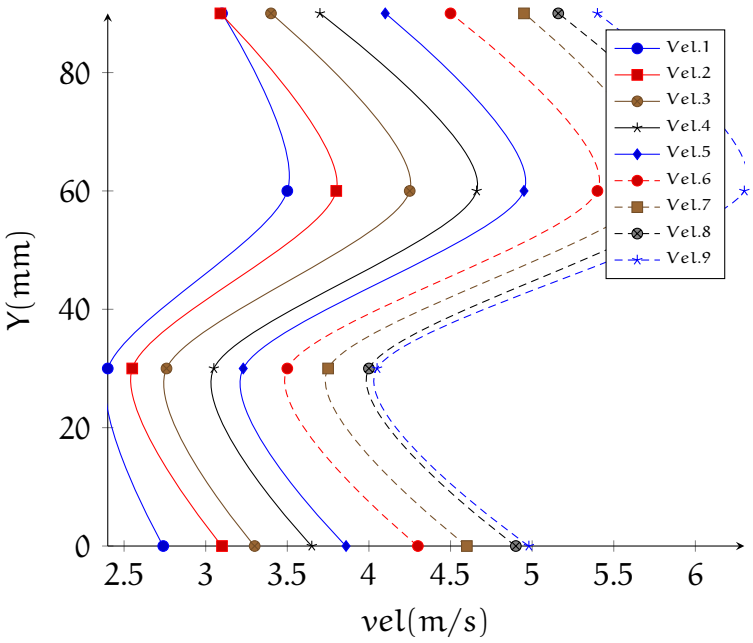

Figure 15: 1st Blower Speed-profile, radius vs velocity

Observing Figure 15 we observe a strong velocity variation over the half cross-section of the cube, even after different improvements [Figure 12] no homogeneous flow could be granted. For this reason a stronger blower substituted the first one.

2nd Blower

The second and definitive blower [Figure 16] generates a flow velocity of over 11m/s ideal for the experiments. Due to the different method of construction this blower showed from the beginning an homogeneous flow. After first tests, using the same process and points as for the first test [Figure 13,Figure 14], a uniform flow at the input section could be confirmed.
The velocity of the input flow was controlled by varying the air-inlet opening. Three different velocities were used in the experiment:

- $V_1 = 50\%$ open.
- $V_2 = 75\%$ open.
- $V_3 = 100\%$ open.

Figure 16: 2nd blower

4.1.5 *Rigid- and Flexible Plates*

The "heart" of the testrig is without any doubt the flexible- and rigid-plate [Figure 17]. The flexible part is made out of silastic3481 a 2 component silicone. To create different plates, a negative mold [Figure 18] was built with a CNC machine. With this mold different exact copies were reproduced. The first tests showed that the silicone used had a high density (1200kg/m3) making it difficult to get it flap. So different models with different thicknesses were made. One of the models was reinforced every 2cm with 0.8mm thick steel wires parallel to the Y direction to avoid three-dimensional movement.

Typical properties of the silicon (Silastic 3481) are:

- Hardness (ShoreA) 21
- Tensile strength 4.9Mpa
- Elongation at break 560%
- Tear strength 26kN/m
- Density 1213kg/m^3
- $E = 1 \times 10^6$Pa (estimate)
- $\nu = 0.03$ (estimate)

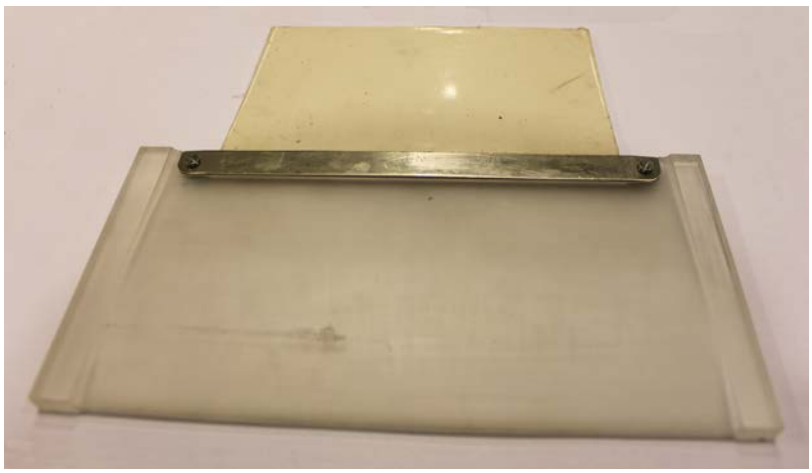

Figure 17: Flexible- and rigid plates

Figure 18: Negative Mold

In total 4 flexible part were build [Figure 19]:

1. equal thickness, very heavy, not enough oscillation for tests.
2. slight thickness variation (connection point > end point), good results.
3. strong thickness vriation (connection point > > end point), silicone not hardening, not usable.
4. like 2 but with 0.5mm wire to guarantee 2-dimensional oscillation, good results.

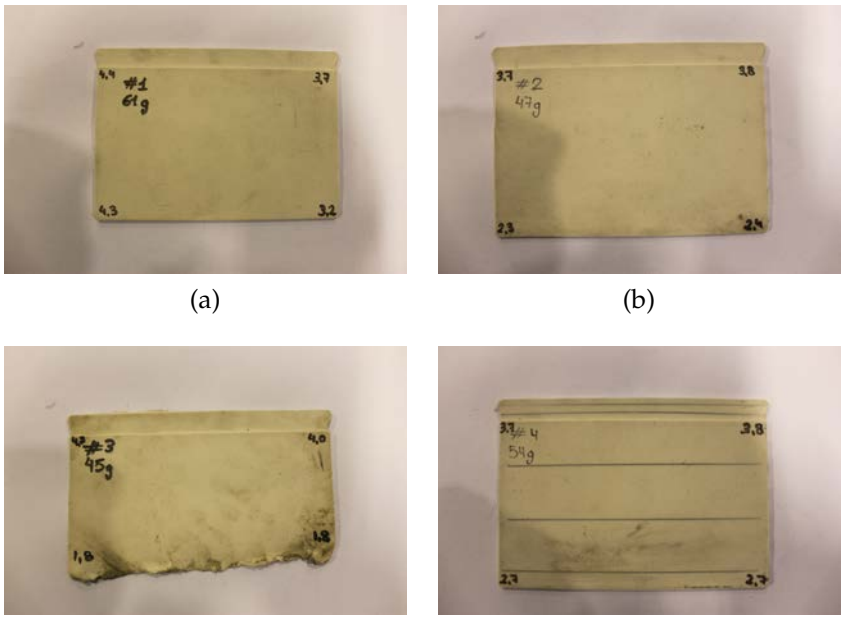

(a) (b)

(c) (d)

Figure 19: Flexible Plates

The rigid plate [Figure 20] was build of 8mm plexiglass. The main function is to sustain the flexible part on one side . It was designed as a symmetrical airfoil [Figure 21, Table 2] to ensure a uniform flow over the rigid-plate, reducing the influence over the flexible plate (possible turbulence). At the trailing edge a connection mechanism for the flapping part was designed. The rigid plate was build completely with a CNC machine to ensure perfect symmetrical flow over the airfoil.

Figure 20: Rigid plate

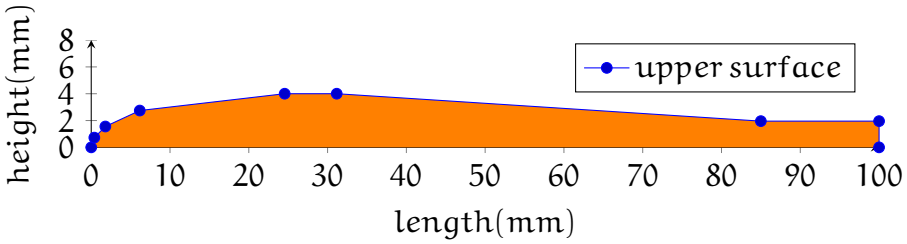

Figure 21: Upper Surface Rigid Plate

Table 2: Rigid plate surface f(x)

X(mm)	f(X)(mm)
0,00	0,00
0,39	0,73
1,79	1,56
6,16	2,75
24,55	4,00
31,16	4,00
85,00	1,96
100,00	1,96
100,00	0,00

4.2 INSTRUMENTATION

For the measurements different kind of pitot-tubes (standart and special Boundary Layer pitot tubes) and a highspeed-camera [Figure 24] were used. To be able to position the pitot-tubes exactly in the testrig a 2-D positioning system [Figure 22] was used.

Figure 22: 2-D Positioning System

The pitot-tube is connected to a transducer and a amplifier, from the amplifier the signal goes to a DAQ [Figure 23] and from their the values are stored and used in the computer.

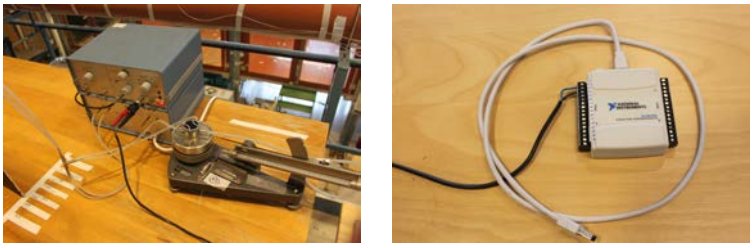

(a) Transducer and amplifier (b) DAQ

Figure 23: Instruments

Figure 24: Fastcam sa1.1

Part III

EXPERIMENTS AND RESULTS

The third part gives insight into the experimentation and the results obtained during the experimentation.

5

THE EXPERIMENTS

5.1 CALIBRATIONS

To ensure high-quality experimental data, it is crucial to provide a uniform and homogeneous inlet flow to the test-rig. A homogeneous flow is important to obtain constant and repeatable measurements and to obtain well defined flow over the flexible part. Pitot-tubes were used to measure the pressure field .

5.1.1 *How to calibrate the instruments*

To get valuable pressure measurements, a pitot-tube has been connected to a transducer, which is connected itself to an amplifier and then to a data acquisition card (DAQ)[Figure 23]. The DAQ gives continuous output information which can than be transformed to pressure and velocity information.

To ensure a correct correlation between pressure and voltage, a first calibration is of need. Using a manual Manometer switched in parallel to the pitot-tube and the transducer [Figure 25] different velocities were measured at a random point insight the cube, obtaining a linear regression. This correlation is than used to get pressure information from the voltage input of the DAQ.

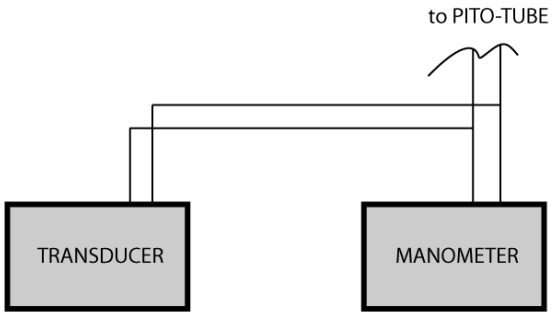

Figure 25: Sketch Manometer Transducer

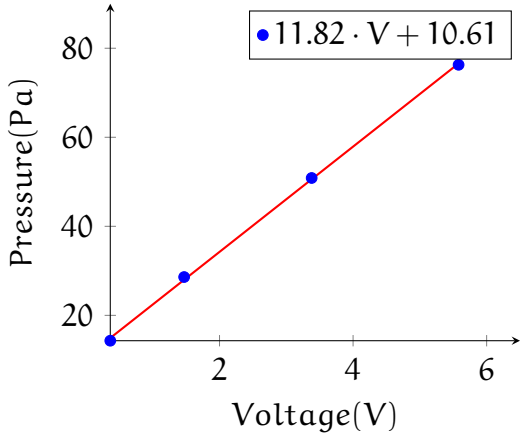

Figure 26: Calibration Transducer

5.1.2 *The endless way to calibrate the testrig*

After calibrating the pressure sensors, the next step is to verify a homogeneous and uniform input-flow. For this, several test-measurements are needed. Using the coordinate-system shown in the figure [Figure 27, Figure 28], the first measurements were done in the horizontal middle plan in section 3. Observing the first result, it is clear that improvements are necessary. First intents were improving the output flow of the fan reducing the vortex created by the own radial movement of the blower [Figure 12]. After decreasing the vortex effect using guiding blades and a honeycomb the output speed decreases to a value where the flexible part didn't interact with the input flow. A stronger blower with higher end-speed was needed. To ensure a complete development of the speed-profile a 4m flexible pipe has been connected between the blower and the testrig. Between blower and the conduct a fine grid mesh helps to get a more uniform profile over the whole conduct area. It is of high important to align the blower, pipes and testrig to ensure a uniform flow. After calibrating the testrig a standard FSI test should show if the measurements taken in the testrig are useable or not. After days of research, no standard/benchmark FSI test-case was found in the literature. In agreement with the supervisor the decision that no standard FSI test for our testrig is of need.

As shown in the next topic, different sections in transverse (horizontal) and vertical planes were measured, confirming a homogeneous and uniform input-flow. Section 1 is at the Lead-

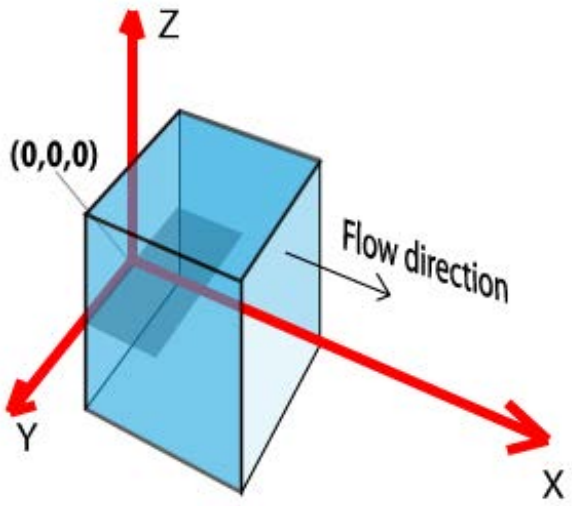

Figure 27: Coordinate-system

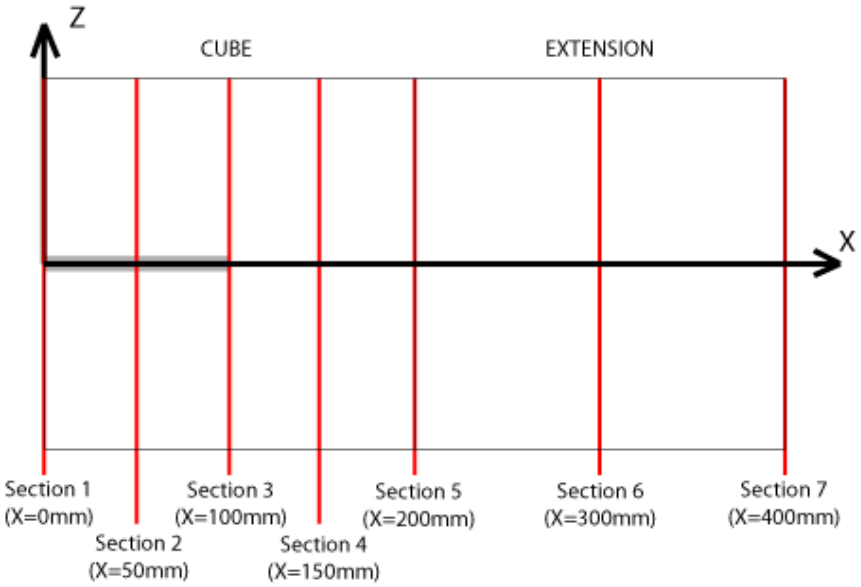

Figure 28: Sections for calibration

ing edge,the distances between Section 1 - 5 is 50mm, the distances between Section 5 - 7 is 100mm. All measurements were taken parallel to the Z-axis and Y = 0 for vertical and parallel to the Y-axis and Z=0 for the horizontal measurements.The first point of each measurement was taken 10 mm from the bottom (vertical measurements) and 10 mm from the right surface watching in x direction (horizontal measurements). All results obtained are listed and explained in the next section.

5.1.3 *Static pressure*

Using pitot tubes in a turbulent system can produce errors in the measurements due to the fact that the velocity field has some vortices, these vortices have an huge influence on the static pressure. To guarantee good results the static pressure has been taken outside of the testrig. Comparing static pressure and atmospheric pressure at different points taken in a transverse plane to the X-axis, with a linear velocity field system and a turbulent system(FSI), both measured with the static pressure taken inside the cube and the atmospheric pressure taken outside, we can confirm that in a linear system the static pressure inside the cube is almost equal (no influence for measurement results) to the atmospheric pressure outside. With turbulent flow we observe a big difference between static- and atmospheric pressure measurement [Table 3,Table 4]. The measurement points inside the cube for the laminar and turbulent tests were the same, the measurement point outside was the same for all measurements. The following tables represent the pressure difference between in-and outside of each measurement point in the YZ plane inside the cube with the random measurement point outside the cube (the calmest place were under the table where the testrig stands). The coordinates of the 9 points are:

- $\mathrm{First\,row}(Z = -87)$: $Mp_1(Y = -87)$, $Mp_2(Y = 0)$, $Mp_3(Y = 87)$.
- $\mathrm{Second\,row}(Z = 0)$: $Mp_4(Y = -87)$, $Mp_5(Y = 0)$, $Mp_6(Y = 87)$.
- $\mathrm{Third\,row}(Z = 87)$: $Mp_7(Y = -87)$, $Mp_8(Y = 0)$, $Mp_9(Y = 87)$.

Table 3: Difference between static pressure inside the test-rig and atmospheric pressure outside at different points at the YZ plane in section 3 [Figure 28], laminar flow. "$\Delta\mathrm{Pressure(Pa)}$", $\mathrm{error_p} = 1.8\mathrm{Pa}$

$-0{,}71$	$-0{,}26$	$0{,}31$
$3{,}28 \cdot 10^{-2}$	$9{,}54 \cdot 10^{-2}$	$0{,}33$
$0{,}43$	$-3{,}52 \cdot 10^{-2}$	$0{,}61$

Table 4: Difference between static pressure inside the test-rig and atmospheric pressure outside at different points at the YZ plane in section 3 [Figure 28], turbulent system "$\Delta Pressure(Pa)$", $error_p = 5.7Pa$"

−2,21	7,53	−0,35
$7{,}73 \cdot 10^{-2}$	5,54	−0,52
2,45	3,61	1,11

5.2 THE EXPERIMENTS

5.2.1 *Flow Experiments*

After initial testing and calibration, the first experiments consists in measuring the pressure and velocity fields with only the rigid-plate inserted. Assuming uniform input flow, the measurements were done along the vertical center-line of each cross section. In total 7 sections are measured[Figure 27]. Each section has 11 points with a distance of 17.5mm between each other in vertical direction. Figure 28 shows the position and distances of the sections. To complete the flow experiment boundary layer measurements were realized. Each one of the measurements were realized at 3 different velocities. Section 1 is at the Leading edge,the distances between Section 1 - 5 is 50mm,the distances between Section 5 - 7 is 100mm. All measurements have been taken parallel to the Z-axis and Y = 0 for vertical and parallel to the Y-axis and Z=0 for the horizontal measurements.The first point of each measurement were taken 10 mm from the bottom

Profile

Pressure and velocity profiles where generated by recording velocity and pressure with 2000 samples/second, for 20 seconds and taking the time-average, to obtain an average value and a standard deviation. The procedure was repeated for all points of all sections with three different inlet flow velocities[Figure 28].

Boundary Layers

Next step was measuring the evolution of the thickness of the boundary layer. Using a special pitot-tube, 2 different sections Figure 29 have been measured. Each section consist of 9 points. To guarantee exact results, the distance between each point in

z direction is 0.5mm. Section BL1 is 27 mm from the Leading edge. Section BL2 is at the trailing edge of the rigid plate. All measurements have been taken parallel to the Z-axis and Y = 0. The first point of each measurement have been taken on the surface of the rigid plate (Z'=0) of each section

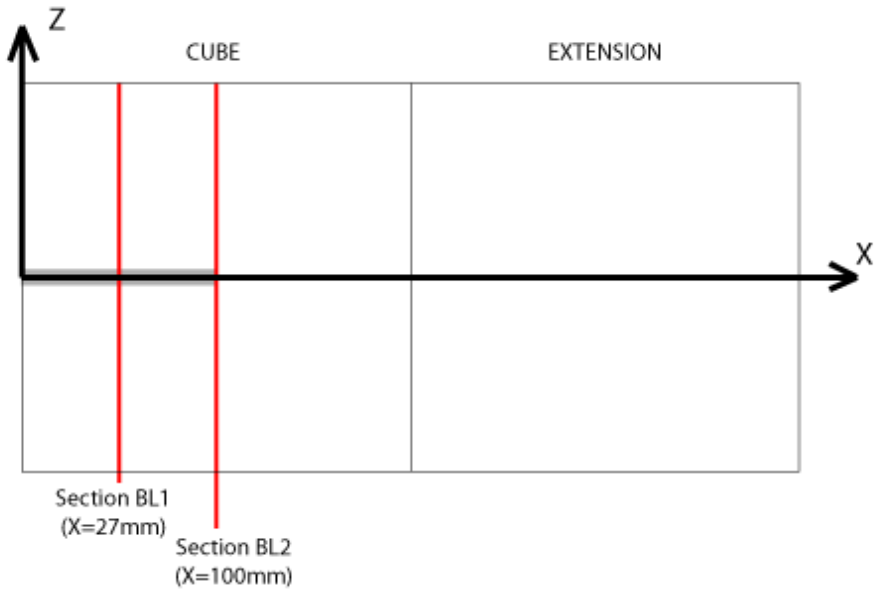

Figure 29: Sections for Boundary Layers

5.2.2 *FSI Experiments*

After measuring the pressure fields in the previous experiments, in this study the flexible part is fixed to the rigid element. With the testrig mounted velocity-field measurements and high-speed-camera records are done.

Profile

Repeating the same process but this time with just 3 sections [Figure 27, Figure 30] as in the studies before, new pressure field measurements have been obtained. For the FSI test 2 different flexible parts are used. Due to the unstable flow each measurement have been taken during 60 seconds to get a valuable average and Standard deviation (std) value.

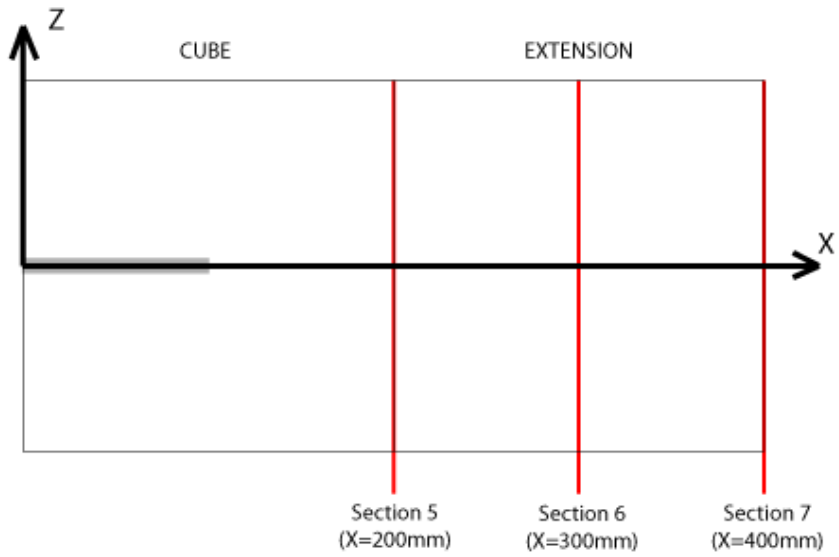

Figure 30: Sections for FSI

High-speed Camera

To complete the FSI study a high-speed camera analysis was realized. Using the fastcam sa.1.2 with 1000 frames per second the oscillating movement for Steady state [Figure 31] and transient state [Figure 32] are recorded. The recordings for steady state movement were taken after the movement of the flexible plate got stable (10 seconds after switching on the fan), and for the transient state the recording started at the same time the blower was turned on. The position of 5 points (10, 35, 50, 65 and 80mm from the leading edge of the flexible plate) on the flexible part were analyzed to determine the dynamics of the flexible plate. To get the movement of the 5 points a image processing software recognized each of the points (black dots at the flexible plates) and followed the movement for each frame. So for each point the X- and Z- position at each frame was calculated. To get the positions in mm a special snapshot of a paper in the cube with a reference length allowed to convert the pixel measurements in mm. For the recordings just V_2 and V_3 were used.

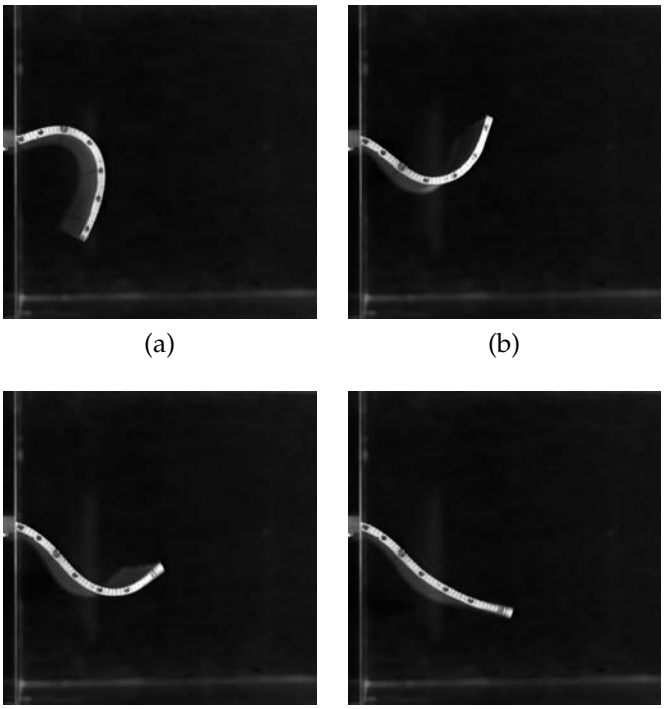

(a) (b)

(c) (d)

Figure 31: Steady state movement of the flexible plate

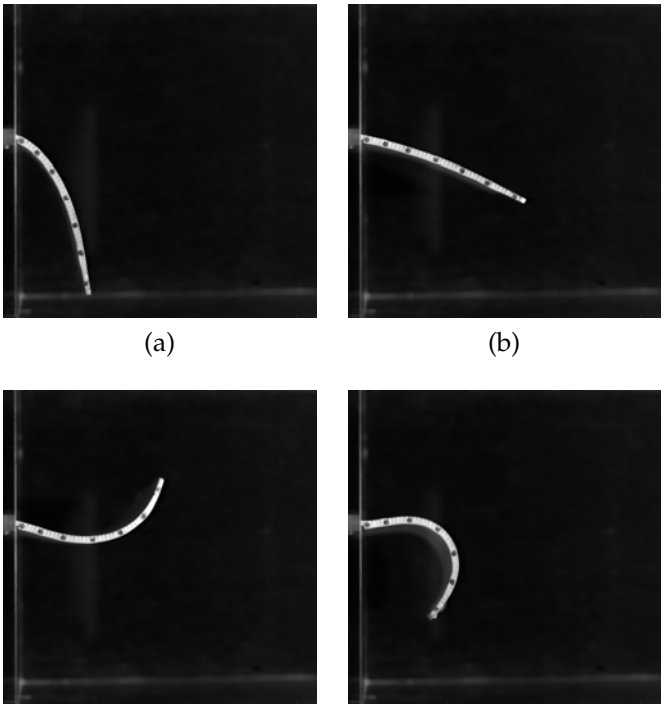

(a) (b)

(c) (d)

Figure 32: Transient state movment of the flexible plate

5.2.3 *Mathematical Modelling*

The industrial modelling tool COMSOL Multiphysics [Figure 33] was used to make a mathematical model of the test-rig, with the flexible part in place. A brief, qualitative comparison between experimental and modelling data was performed (See Section 6.4).

The following values were used for the CFD study:

$$\mathrm{Inlet} : U_0 = 10\mathrm{m/s} \tag{6}$$

$$\mathrm{Outlet} : P_0 = 0\mathrm{Pa} \tag{7}$$

$$T = 293.15\mathrm{K} \tag{8}$$

$$F_t = -0.75\mathrm{N(Y-dir)} \tag{9}$$

$$\mathrm{Silastic3481} : \tag{10}$$

$$\rho_s = 1213\mathrm{kg/m^3} \tag{11}$$

$$E = 1 \times 10^6\mathrm{Pa} \tag{12}$$

$$\nu = 0.03 \tag{13}$$

For the CFD study RANS was used to model the effects of turbulence, free triangular mesh was used for the geometry. The FSI interface uses the ALE method to combine the fluid flow with the solid mechanics. For the numerical solution a fully coupled configuration with Newton nonlinear method and a once per time step jacobian update was used.

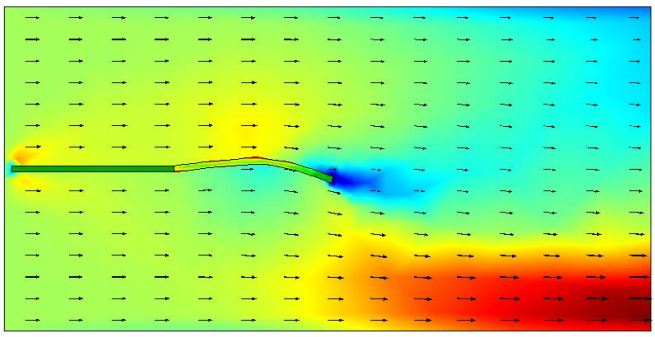

Figure 33: Comsol Graphic Example

6 RESULTS

In this chapter all velocity profile graphics and tables are listed and discussed.Related pressure tables are attached in Section A.6.

6.1 CALIBRATION

In this section all relevant graphics and tables from the calibration are listed and discussed. The calibration measurements were done without rigid- and without flexible plate.

6.1.1 *Graphics*

The first 3 graphics show the "horizontal" Velocity-profile for 3 different velocities with the associated error bars. Horizontal means that the measurement points were taken parallel to the Y-axis at section 1, 2 and 3. Due to some wall effects the first and last measurement were taken 10mm from the walls.
As the flexible plate just measures 142mm in y-direction their was no need to guaranty uniform flow at wall regions.

Comparing all 3 graphics [Figure 37] a stable flow for all 3 velocity can be observed. The velocity keeps constant +-0.5m/s over more than 150mm for all 3 sections at each speed With this conclusion we can guarantee a uniform and homogeneous horizontal inlet flow at Z=0 from Y=-75mm to Y= 75mm.

For this first meaurements the rigid plate was not placed in the cube.

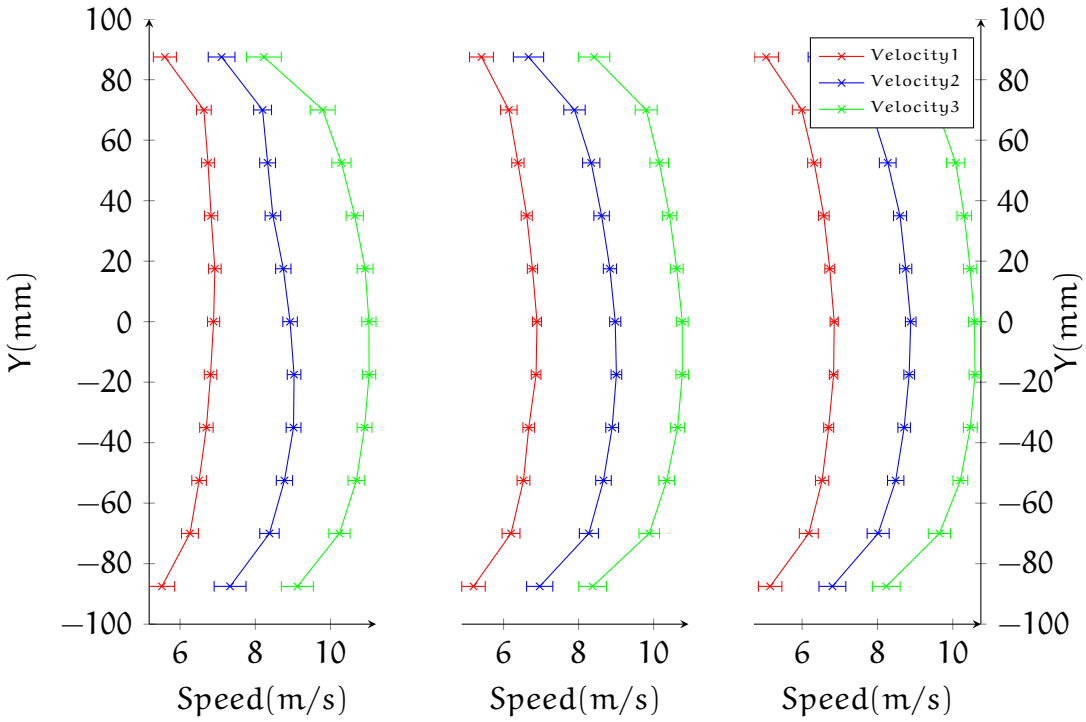

Figure 34: Section 1 Figure 35: Section 2 Figure 36: Section 3

Figure 37: Calibration curves, horizontal (Z=0) (see Section 5.1.2 for information about section positioning)

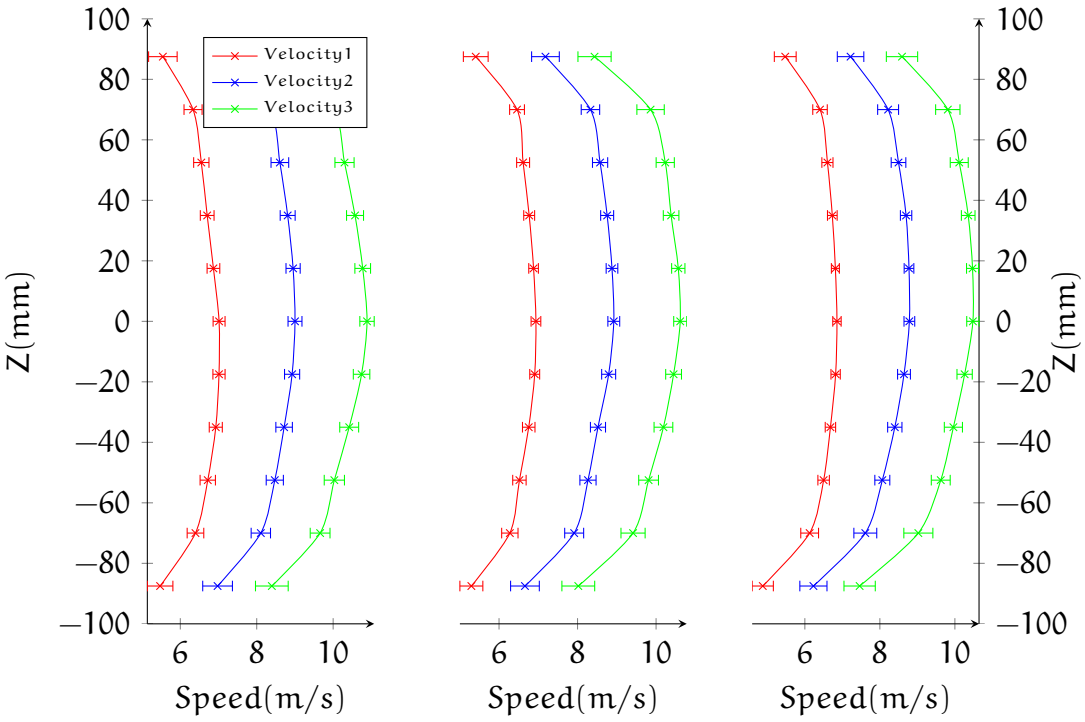

Figure 38: Section 1 Figure 39: Section 2 Figure 40: Section 3

Figure 41: Calibration curves, Vertical (Y=0) (see Section 5.1.2 for information about section positioning)

Equal as for the horizontal measurements, the vertical measurements had to be uniform and homogeneous too. 3 graphics [Figure 41] show the "Vertical" Velocity-profile for 3 different velocities with the associated error bars. Vertical means that the measurement points were taken parallel to the Z-axis at section 1, 2 and 3. Due to some wall effects the first and last measurement were taken 10mm from the walls. The flexible plate can just move +-80mm maximum in Z-direction (in the experiments never more than 60mm), due to it's geometry, their was no need to guaranty uniform flow at the upper and lower wall regions. Comparing all 3 graphics a stable flow for all 3 velocity can be observed. The velocity keeps constant +-0.5m/s over more than 120mm for all 3 sections at each speed. With this conclusion we can guarantee a uniform and homogeneous vertical inlet flow at Y=0 from Z=-60mm to Z= 60mm. Observing the results for horizontal and vertical measurements a homogeneous and uniform inlet-flow for high quality experiments can be granted for the whole testrig.

6.1.2 *Tables*

The following tables show the numerical part of the graphics explained in the upper section. Each table contains the speed and the associated error for each measurement point and fan-velocity.

Table 5: Calibration Section 1 Horizontal

Y(mm)	$V_1(m/s)$	$e_1(m/s)$	$V_2(m/s)$	$e_2(m/s)$	$V_3(m/s)$	$e_3(m/s)$
−87,5	5,517	0,339	7,330	0,424	9,120	0,426
−70,0	6,263	0,225	8,377	0,258	10,239	0,283
−52,5	6,506	0,194	8,776	0,216	10,690	0,223
−35,0	6,700	0,178	9,018	0,197	10,906	0,197
−17,5	6,810	0,165	9,031	0,180	11,026	0,177
0,0	6,891	0,161	8,925	0,193	11,022	0,190
17,5	6,925	0,167	8,745	0,204	10,921	0,211
35,0	6,825	0,176	8,468	0,207	10,646	0,229
52,5	6,742	0,169	8,328	0,211	10,292	0,255
70,0	6,632	0,196	8,194	0,238	9,793	0,331
87,5	5,596	0,306	7,104	0,356	8,228	0,464

Table 6: Calibration Section 1 Vertical

Z(mm)	$V_1(m/s)$	$e_1(m/s)$	$V_2(m/s)$	$e_2(m/s)$	$V_3(m/s)$	$e_3(m/s)$
−87,5	5,472	0,334	6,976	0,389	8,396	0,428
−70,0	6,397	0,217	8,107	0,253	9,659	0,259
−52,5	6,719	0,201	8,473	0,225	10,031	0,265
−35,0	6,929	0,171	8,717	0,216	10,420	0,247
−17,5	7,013	0,159	8,926	0,198	10,744	0,216
0,0	7,015	0,156	9,002	0,182	10,887	0,188
17,5	6,867	0,166	8,952	0,186	10,774	0,205
35,0	6,704	0,180	8,810	0,196	10,573	0,222
52,5	6,550	0,200	8,606	0,231	10,298	0,251
70,0	6,334	0,236	8,355	0,264	10,023	0,289
87,5	5,544	0,374	7,168	0,395	8,794	0,444

Table 7: Calibration Section 2 Horizontal

Y(mm)	$V_1(m/s)$	$e_1(m/s)$	$V_2(m/s)$	$e_2(m/s)$	$V_3(m/s)$	$e_3(m/s)$
−87,5	5,198	0,314	6,963	0,350	8,374	0,371
−70,0	6,198	0,239	8,275	0,255	9,883	0,273
−52,5	6,530	0,170	8,664	0,207	10,349	0,210
−35,0	6,671	0,155	8,895	0,170	10,640	0,186
−17,5	6,866	0,129	9,008	0,142	10,764	0,169
0,0	6,891	0,120	8,977	0,148	10,764	0,157
17,5	6,770	0,136	8,835	0,175	10,618	0,171
35,0	6,617	0,148	8,614	0,206	10,426	0,193
52,5	6,382	0,163	8,336	0,230	10,151	0,248
70,0	6,139	0,220	7,891	0,285	9,803	0,293
87,5	5,411	0,318	6,664	0,404	8,413	0,418

Table 8: Calibration Section 2 Vertical

Z(mm)	$V_1(m/s)$	$e_1(m/s)$	$V_2(m/s)$	$e_2(m/s)$	$V_3(m/s)$	$e_3(m/s)$
−87,5	5,295	0,292	6,660	0,366	8,019	0,418
−70,0	6,275	0,208	7,914	0,242	9,414	0,308
−52,5	6,519	0,171	8,266	0,206	9,810	0,252
−35,0	6,757	0,159	8,520	0,192	10,187	0,239
−17,5	6,909	0,126	8,792	0,178	10,446	0,201
0,0	6,940	0,124	8,923	0,151	10,615	0,166
17,5	6,880	0,123	8,877	0,148	10,566	0,169
35,0	6,768	0,139	8,754	0,165	10,383	0,199
52,5	6,613	0,165	8,574	0,193	10,233	0,232
70,0	6,458	0,189	8,328	0,235	9,860	0,349
87,5	5,407	0,316	7,183	0,353	8,433	0,423

Table 9: Calibration Section 3 Horizontal

Y(mm)	$V_1(m/s)$	$e_1(m/s)$	$V_2(m/s)$	$e_2(m/s)$	$V_3(m/s)$	$e_3(m/s)$
−87,5	5,152	0,311	6,804	0,356	8,234	0,368
−70,0	6,178	0,251	8,019	0,293	9,645	0,295
−52,5	6,530	0,176	8,484	0,217	10,201	0,196
−35,0	6,705	0,133	8,709	0,166	10,465	0,183
−17,5	6,836	0,113	8,842	0,140	10,589	0,156
0,0	6,852	0,108	8,883	0,141	10,577	0,163
17,5	6,735	0,131	8,751	0,160	10,462	0,176
35,0	6,576	0,141	8,599	0,173	10,304	0,194
52,5	6,320	0,173	8,273	0,222	10,076	0,242
70,0	5,993	0,253	7,835	0,300	9,589	0,341
87,5	5,047	0,324	6,535	0,375	8,644	0,435

Table 10: Calibration Section 3 Vertical

Z(mm)	$V_1(m/s)$	$e_1(m/s)$	$V_2(m/s)$	$e_2(m/s)$	$V_3(m/s)$	$e_3(m/s)$
−87,5	4,878	0,282	6,228	0,362	7,460	0,417
−70,0	6,128	0,237	7,612	0,305	9,026	0,387
−52,5	6,500	0,153	8,065	0,200	9,623	0,252
−35,0	6,682	0,138	8,398	0,191	9,960	0,242
−17,5	6,820	0,124	8,643	0,171	10,260	0,204
0,0	6,856	0,112	8,786	0,143	10,480	0,164
17,5	6,814	0,107	8,777	0,129	10,470	0,160
35,0	6,732	0,129	8,699	0,152	10,355	0,182
52,5	6,602	0,148	8,497	0,195	10,116	0,240
70,0	6,404	0,193	8,220	0,279	9,811	0,325
87,5	5,477	0,291	7,219	0,353	8,590	0,417

6.2 FLOW MEASUREMENTS

In this section all relevant graphics and tables from the flow experiments are listed.

6.2.1 *Profile*

Graphics

After confirming a homogeneous and uniform inlet-flow, first flow experiments with the rigid part inserted were realized. For the next experiments only the vertical measurement points were taken, since this are the only relevant measurement points, supposing 2-D movement (no 3-Dimensional effects are taken in account). Observing the first 3 plots[Figure 42, Figure 43, Figure 44] we can see that the flow is even more stable than without the rigid-plate.
As it is logical the velocity decreases to om/s for all 3 velocities and the first 3 sections at Z=0, as at this Z-position the rigid-plate is fixed. In section 4 a the velocity-profile starts to recover its original profile. Observing sections 4 to 7 the profile recovers slowly to its normal profile. Section 7 has almost recovered the original profile. As for the CFD-validations more exact information was needed, Boundary Layer Measurements were taken to complete the flow experiments (see section Boundary Layers).

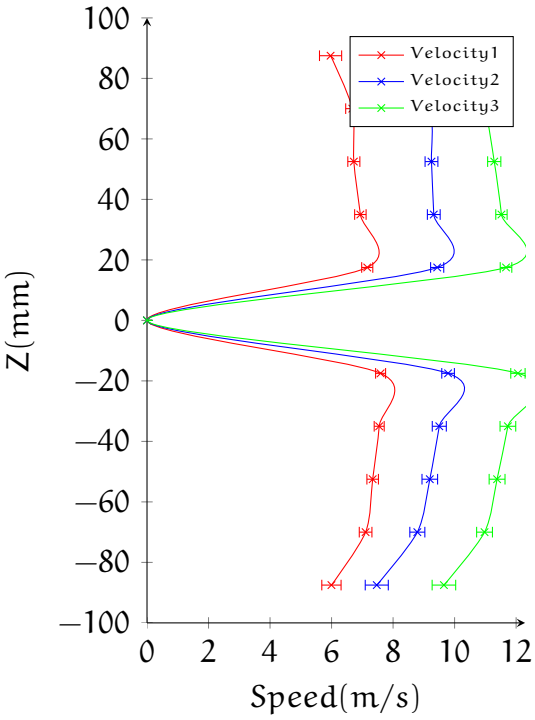

Figure 42: Flow Section 1

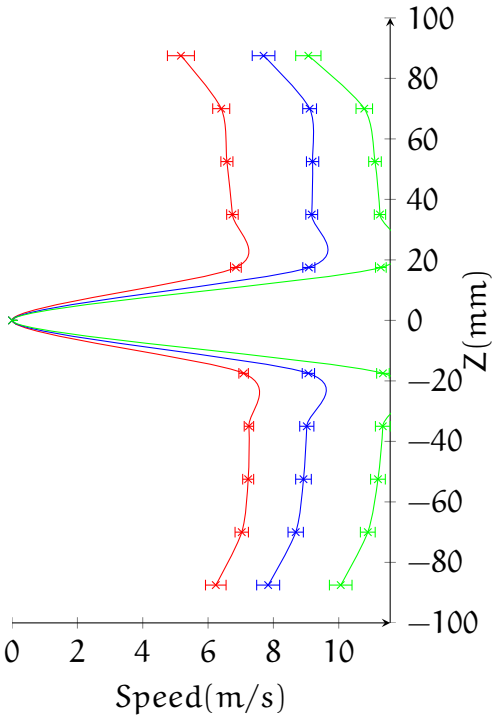

Figure 43: Flow Section 2

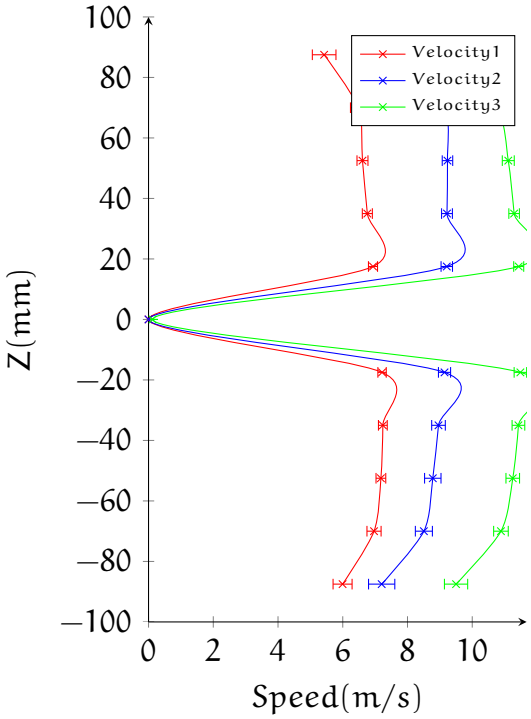

Figure 44: Flow Section 3

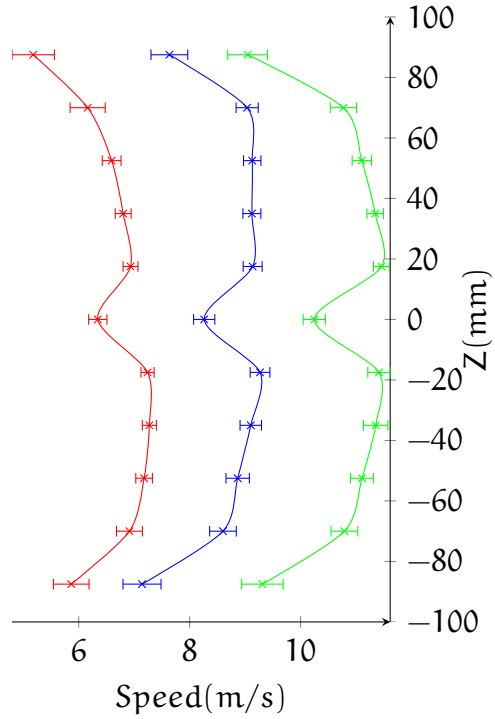

Figure 45: Flow Section 4

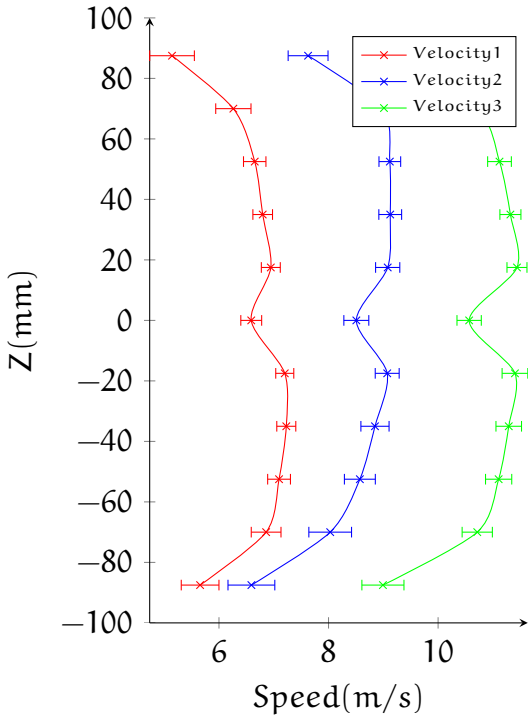

Figure 46: Flow Section 5

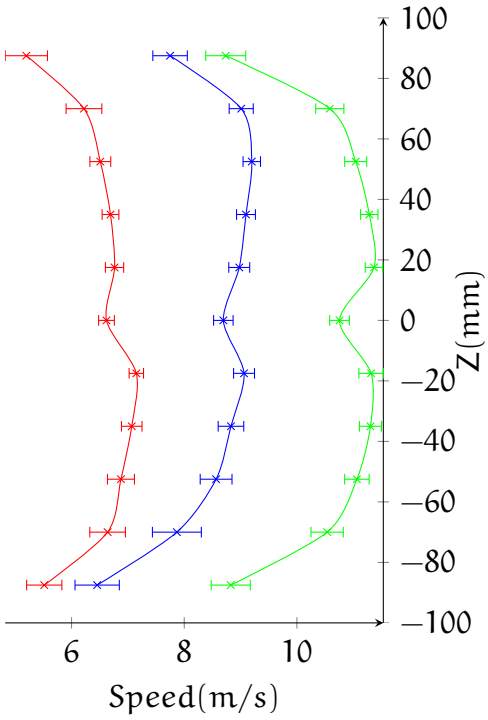

Figure 47: Flow Section 6

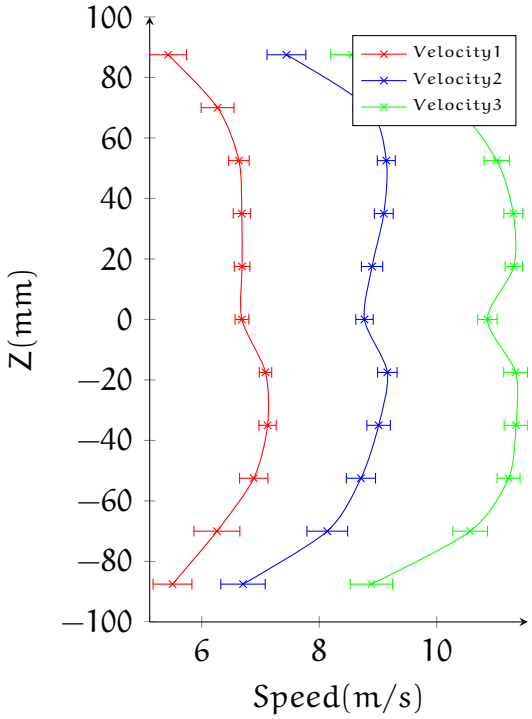

Figure 48: Flow Section 7

Tables

The following tables show the numerical part of the graphics explained in the upper section. Each table contains the speed and the associated error for each measurement point and fan-velocity.

Table 11: Flow Section 1

Z(mm)	$V_1(m/s)$	$e_1(m/s)$	$V_2(m/s)$	$e_2(m/s)$	$V_3(m/s)$	$e_3(m/s)$
−87,5	5,996	0,313	7,470	0,375	9,653	0,383
−70,0	7,107	0,206	8,789	0,244	10,974	0,257
−52,5	7,336	0,187	9,194	0,254	11,381	0,258
−35,0	7,548	0,162	9,503	0,228	11,733	0,255
−17,5	7,594	0,162	9,788	0,205	12,059	0,233
0,0	0,000	0,000	0,000	0,000	0,000	0,000
17,5	7,160	0,181	9,434	0,214	11,672	0,188
35,0	6,937	0,186	9,323	0,208	11,523	0,184
52,5	6,724	0,196	9,249	0,208	11,289	0,215
70,0	6,675	0,215	9,166	0,220	10,958	0,236
87,5	5,968	0,360	7,825	0,383	10,064	0,351

Table 12: Flow Section 2

Z(mm)	$V_1(m/s)$	$e_1(m/s)$	$V_2(m/s)$	$e_2(m/s)$	$V_3(m/s)$	$e_3(m/s)$
−87,5	6,236	0,315	7,839	0,352	10,061	0,346
−70,0	7,031	0,205	8,683	0,235	10,890	0,227
−52,5	7,228	0,168	8,921	0,240	11,201	0,226
−35,0	7,251	0,144	9,022	0,217	11,349	0,226
−17,5	7,089	0,145	9,071	0,188	11,353	0,193
0,0	0,000	0,000	0,000	0,000	0,000	0,000
17,5	6,852	0,164	9,085	0,185	11,289	0,163
35,0	6,746	0,177	9,174	0,181	11,262	0,173
52,5	6,577	0,184	9,200	0,188	11,110	0,193
70,0	6,403	0,260	9,109	0,211	10,782	0,253
87,5	5,169	0,413	7,699	0,347	9,069	0,387

Table 13: Flow Section 3

Z(mm)	$V_1(m/s)$	$e_1(m/s)$	$V_2(m/s)$	$e_2(m/s)$	$V_3(m/s)$	$e_3(m/s)$
−87,5	5,994	0,294	7,202	0,405	9,500	0,359
−70,0	6,966	0,218	8,506	0,263	10,887	0,226
−52,5	7,178	0,150	8,781	0,254	11,252	0,210
−35,0	7,239	0,136	8,958	0,211	11,427	0,196
−17,5	7,214	0,130	9,144	0,188	11,487	0,193
0,0	$3{,}575 \cdot 10^{-5}$	0,000	0,000	0,000	0,126	0,000
17,5	6,934	0,140	9,214	0,177	11,436	0,155
35,0	6,759	0,155	9,220	0,167	11,294	0,163
52,5	6,609	0,169	9,235	0,162	11,113	0,185
70,0	6,478	0,240	9,165	0,191	10,770	0,236
87,5	5,425	0,365	8,009	0,345	9,238	0,383

Table 14: Flow Section 4

Z(mm)	$V_1(m/s)$	$e_1(m/s)$	$V_2(m/s)$	$e_2(m/s)$	$V_3(m/s)$	$e_3(m/s)$
−87,5	5,865	0,321	7,141	0,343	9,311	0,375
−70,0	6,915	0,234	8,600	0,240	10,790	0,241
−52,5	7,179	0,150	8,866	0,211	11,107	0,209
−35,0	7,273	0,127	9,102	0,193	11,354	0,220
−17,5	7,240	0,118	9,269	0,178	11,413	0,202
0,0	6,344	0,165	8,262	0,191	10,247	0,200
17,5	6,934	0,134	9,136	0,171	11,459	0,144
35,0	6,801	0,143	9,122	0,162	11,345	0,149
52,5	6,594	0,169	9,128	0,157	11,104	0,175
70,0	6,161	0,316	9,036	0,200	10,772	0,237
87,5	5,180	0,382	7,634	0,331	9,045	0,359

Table 15: Flow Section 5

Z(mm)	V_1(m/s)	e_1(m/s)	V_2(m/s)	e_2(m/s)	V_3(m/s)	e_3(m/s)
−87,5	5,656	0,344	6,592	0,427	8,993	0,384
−70,0	6,861	0,271	8,030	0,390	10,715	0,276
−52,5	7,097	0,208	8,572	0,282	11,105	0,239
−35,0	7,229	0,174	8,848	0,257	11,290	0,233
−17,5	7,201	0,165	9,071	0,218	11,403	0,234
0,0	6,589	0,190	8,507	0,228	10,567	0,222
17,5	6,946	0,173	9,080	0,221	11,440	0,182
35,0	6,798	0,179	9,126	0,208	11,320	0,192
52,5	6,652	0,205	9,119	0,198	11,121	0,216
70,0	6,263	0,322	8,981	0,242	10,706	0,279
87,5	5,143	0,408	7,627	0,364	8,988	0,409

Table 16: Flow Section 6

Z(mm)	V_1(m/s)	e_1(m/s)	V_2(m/s)	e_2(m/s)	V_3(m/s)	e_3(m/s)
−87,5	5,515	0,312	6,455	0,393	8,826	0,347
−70,0	6,640	0,316	7,870	0,434	10,536	0,287
−52,5	6,877	0,240	8,566	0,282	11,065	0,217
−35,0	7,068	0,183	8,829	0,227	11,306	0,196
−17,5	7,150	0,128	9,062	0,186	11,317	0,217
0,0	6,620	0,140	8,694	0,173	10,756	0,174
17,5	6,763	0,162	8,977	0,186	11,369	0,156
35,0	6,691	0,149	9,096	0,167	11,285	0,154
52,5	6,510	0,185	9,199	0,155	11,044	0,195
70,0	6,220	0,317	9,011	0,214	10,584	0,250
87,5	5,197	0,375	7,749	0,306	8,737	0,355

Table 17: Flow Section 7

Z(mm)	V_1(m/s)	e_1(m/s)	V_2(m/s)	e_2(m/s)	V_3(m/s)	e_3(m/s)
−87,5	5,504	0,331	6,703	0,378	8,887	0,359
−70,0	6,260	0,390	8,137	0,346	10,570	0,295
−52,5	6,886	0,241	8,710	0,248	11,222	0,195
−35,0	7,121	0,147	9,011	0,200	11,348	0,201
−17,5	7,086	0,106	9,159	0,166	11,342	0,202
0,0	6,685	0,117	8,771	0,148	10,862	0,165
17,5	6,687	0,133	8,899	0,181	11,312	0,150
35,0	6,683	0,146	9,099	0,161	11,302	0,161
52,5	6,634	0,175	9,141	0,153	11,020	0,215
70,0	6,271	0,280	8,834	0,258	10,294	0,339
87,5	5,429	0,313	7,442	0,330	8,557	0,362

6.2.2 *Boundary Layers*

Graphics

For detailed velocity-profiles at the airfoil region, Boundary layer measurements were taken. The following graphics show the speed evolution from the top of the rigid plate to it's complete evolution.
2 Boundary layer section were measured as explained in Section 5.2.1. Observing graphic Figure 49 the boundary layer has an height of aprox 1.5mm for all 3 velocities and graphic Figure 50 aprox 1.8mm.
Theoretically the velocity at $Z' = 0$ should be om/s, observing Figure 49 and Figure 50 the velocity at $Z' = 0$ is >om/s this is due to the effect that the air inlet of the boundary layer pitot tube has an diameter of 0.7mm, that causes an inexactitude in the measurement.

At the end of the rigid plate, the Reynolds number is about 14666.

$$u = 11 m/s \tag{14}$$

$$\nu = 1.5 \times 10^{-5} m^2/s \tag{15}$$

$$L = 0.2 m \tag{16}$$

That suggests laminar flow supposing that the freestream turbulence level is less than about 1 percent [17].

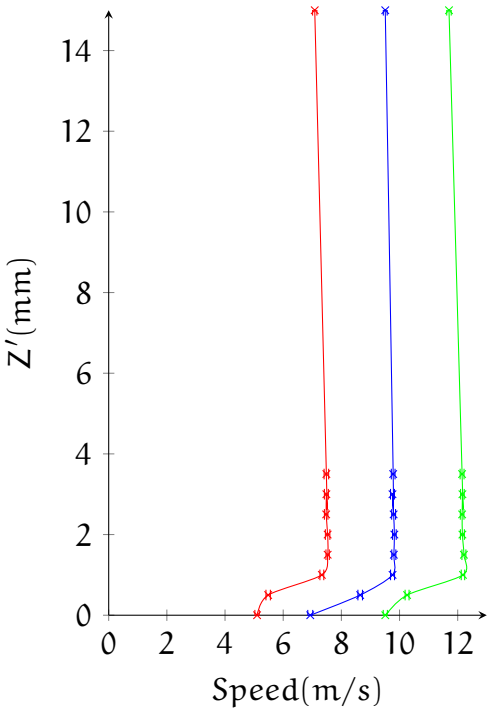

Figure 49: Section BL1

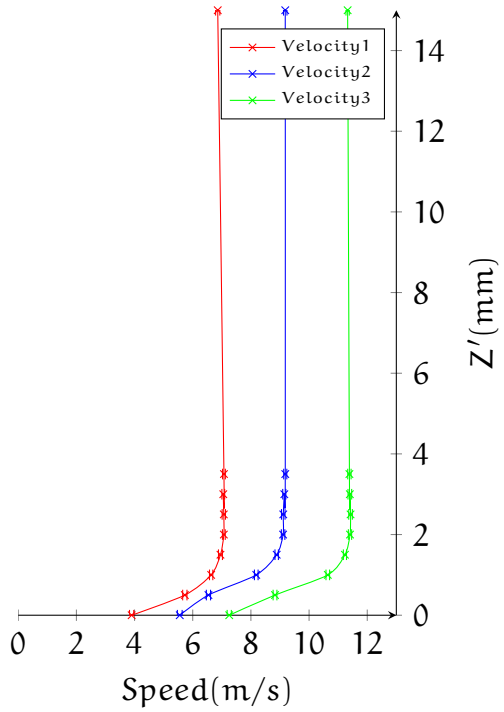

Figure 50: Section BL2

Figure 51: Boundary Layer curves, Vertical (Y=0) (see Section 5.2.1 for information about section positioning)

Tables

The following tables show the numerical part of the graphics explained in the upper section. Each table contains the speed and the associated error for each measurement point and fan-velocity.

Table 18: Boundary Layer, Section BL1

$Z'(mm)$	$V_1(m/s)$	$e_1(m/s)$	$V_2(m/s)$	$e_2(m/s)$	$V_3(m/s)$	$e_3(m/s)$
0,0	5,102	$7{,}621 \cdot 10^{-2}$	6,930	$8{,}521 \cdot 10^{-2}$	9,511	$7{,}102 \cdot 10^{-2}$
0,5	5,484	$7{,}634 \cdot 10^{-2}$	8,648	$7{,}846 \cdot 10^{-2}$	10,260	$6{,}782 \cdot 10^{-2}$
1,0	7,329	$6{,}662 \cdot 10^{-2}$	9,760	$6{,}863 \cdot 10^{-2}$	12,181	$5{,}916 \cdot 10^{-2}$
1,5	7,528	$5{,}747 \cdot 10^{-2}$	9,804	$6{,}961 \cdot 10^{-2}$	12,214	$6{,}835 \cdot 10^{-2}$
2,0	7,528	$7{,}668 \cdot 10^{-2}$	9,823	$6{,}326 \cdot 10^{-2}$	12,161	$6{,}82 \cdot 10^{-2}$
2,5	7,478	$6{,}076 \cdot 10^{-2}$	9,797	$6{,}69 \cdot 10^{-2}$	12,153	$6{,}257 \cdot 10^{-2}$
3,0	7,485	$6{,}813 \cdot 10^{-2}$	9,757	$6{,}727 \cdot 10^{-2}$	12,162	$6{,}232 \cdot 10^{-2}$
3,5	7,485	$7{,}802 \cdot 10^{-2}$	9,782	$6{,}384 \cdot 10^{-2}$	12,151	$6{,}71 \cdot 10^{-2}$
15,0	7,084	$7{,}384 \cdot 10^{-2}$	9,509	$6{,}639 \cdot 10^{-2}$	11,701	$7{,}691 \cdot 10^{-2}$

Table 19: Boundary Layer Section BL2

$Z'(mm)$	$V_1(m/s)$	$e_1(m/s)$	$V_2(m/s)$	$e_2(m/s)$	$V_3(m/s)$	$e_3(m/s)$
0,0	3,899	$7{,}266 \cdot 10^{-2}$	5,554	$8{,}174 \cdot 10^{-2}$	7,255	$7{,}174 \cdot 10^{-2}$
0,5	5,728	$7{,}389 \cdot 10^{-2}$	6,541	$7{,}191 \cdot 10^{-2}$	8,829	$6{,}55 \cdot 10^{-2}$
1,0	6,634	$5{,}731 \cdot 10^{-2}$	8,184	$6{,}276 \cdot 10^{-2}$	10,644	$6{,}203 \cdot 10^{-2}$
1,5	6,953	$6{,}78 \cdot 10^{-2}$	8,887	$5{,}843 \cdot 10^{-2}$	11,233	$5{,}443 \cdot 10^{-2}$
2,0	7,069	$4{,}852 \cdot 10^{-2}$	9,107	$6{,}066 \cdot 10^{-2}$	11,407	$5{,}648 \cdot 10^{-2}$
2,5	7,068	$5{,}695 \cdot 10^{-2}$	9,113	$6{,}106 \cdot 10^{-2}$	11,426	$6{,}21 \cdot 10^{-2}$
3,0	7,051	$4{,}82 \cdot 10^{-2}$	9,149	$5{,}366 \cdot 10^{-2}$	11,402	$6{,}294 \cdot 10^{-2}$
3,5	7,073	$4{,}838 \cdot 10^{-2}$	9,182	$5{,}35 \cdot 10^{-2}$	11,387	$5{,}75 \cdot 10^{-2}$
15,0	6,859	$7{,}252 \cdot 10^{-2}$	9,181	$5{,}965 \cdot 10^{-2}$	11,326	$5{,}708 \cdot 10^{-2}$

6.3 FSI

In this section all relevant graphics and tables from the FSI experiments are listed. To get an better impression of the experiments realized two videos of the FSI highspeed recording are available online [6] and [7].

6.3.1 *Profile, reinforced*

Graphics

Figure 55 show the average value of the turbulent velocity profile for 3 section behind the flexible part. In this section the reinforced flexible part (#4 see Figure 19) was used.
All 3 section [Figure 55] are showing a clear gravity effect from the flexible part. This is due to the weight of the flexible part provoking that the flag moves asymmetrical respect to the Z=0 plane. The movement of the flexible part produces a decrease of the velocity in the area where it oscillates and an increase of the velocity in the rest of the section. Observing section 1 with higher velocity more decreases the velocity in the area where the flag moves. Even with this strong deformation of the velocity profile it recuperates within the 3 section almost completely.
All measurements are time averaged (60 sec).

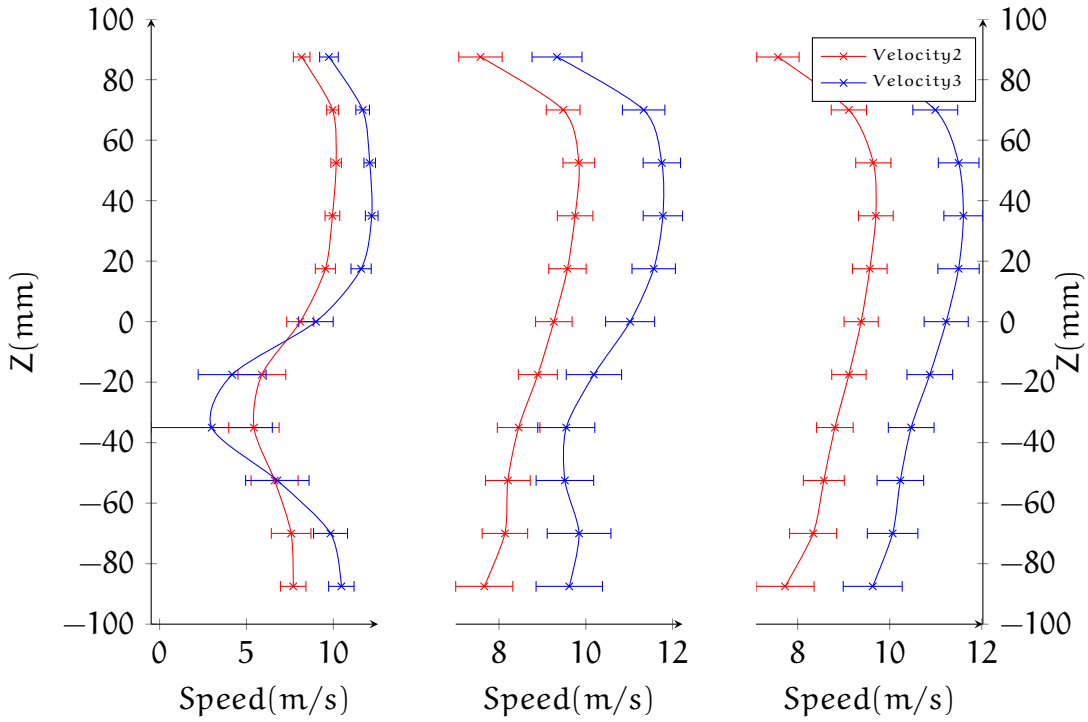

Figure 52: Section 5 Figure 53: Section 6 Figure 54: Section 7

Figure 55: FSI reinforced curves, Vertical (Y=0) (see Section 5.2.2 for information about section positioning)

Tables

Each table contains the speed and the associated error for each measurement point and fan-velocity.

Table 20: FSI reinforced Section 5

Z(mm)	$V_2(m/s)$	$e_2(m/s)$	$V_3(m/s)$	$e_3(m/s)$
−87,5	7,693	0,729	10,462	0,731
−70,0	7,573	1,142	9,841	0,978
−52,5	6,620	1,354	6,778	1,827
−35,0	5,429	1,450	3,002	3,487
−17,5	5,887	1,375	4,176	1,955
0,0	8,097	0,780	9,000	0,994
17,5	9,544	0,577	11,601	0,581
35,0	9,948	0,423	12,211	0,364
52,5	10,162	0,302	12,097	0,331
70,0	9,957	0,338	11,691	0,391
87,5	8,177	0,477	9,749	0,536

Table 21: FSI reinforced Section 6

Z(mm)	$V_2(m/s)$	$e_2(m/s)$	$V_3(m/s)$	$e_3(m/s)$
−87,5	7,661	0,658	9,620	0,765
−70,0	8,136	0,524	9,845	0,734
−52,5	8,205	0,515	9,518	0,663
−35,0	8,453	0,491	9,551	0,657
−17,5	8,895	0,450	10,187	0,638
0,0	9,264	0,421	11,021	0,565
17,5	9,578	0,431	11,566	0,500
35,0	9,754	0,410	11,777	0,454
52,5	9,841	0,365	11,753	0,431
70,0	9,478	0,389	11,334	0,489
87,5	7,573	0,500	9,337	0,575

Table 22: FSI reinforced Section 7

Z(mm)	V_2(m/s)	e_2(m/s)	V_3(m/s)	e_3(m/s)
−87,5	7,727	0,631	9,631	0,641
−70,0	8,336	0,511	10,063	0,549
−52,5	8,569	0,445	10,231	0,506
−35,0	8,809	0,398	10,466	0,497
−17,5	9,114	0,373	10,871	0,496
0,0	9,379	0,371	11,227	0,479
17,5	9,567	0,376	11,495	0,449
35,0	9,698	0,377	11,600	0,424
52,5	9,644	0,382	11,497	0,441
70,0	9,113	0,383	10,989	0,487
87,5	7,572	0,460	9,356	0,560

6.3.2 *Profile, NON reinforced*

Graphics

As with the reinforced flag the velocity decreases at the oscillating area [Figure 59]. For this measurements the standard flexible part (#2 see Figure 19) was used. One difference to the reinforced graphics is the higher position of the area where the velocity decreases. As the reinforced flag is heavier the inlet flow can not elevate the flag as high as the non reinforced flag. The main reason to repeat the measurements with and without reinforcement is to clarify if there is an three-dimensional effect affecting the movement of the flexible plate. In the high-speed recordings it is clearly to see that the reinforced flexible plate moves almost perfect in two-dimensions(XZ plane), while the movement of the non-reinforced flexible plate is nearly 3-dimensional.

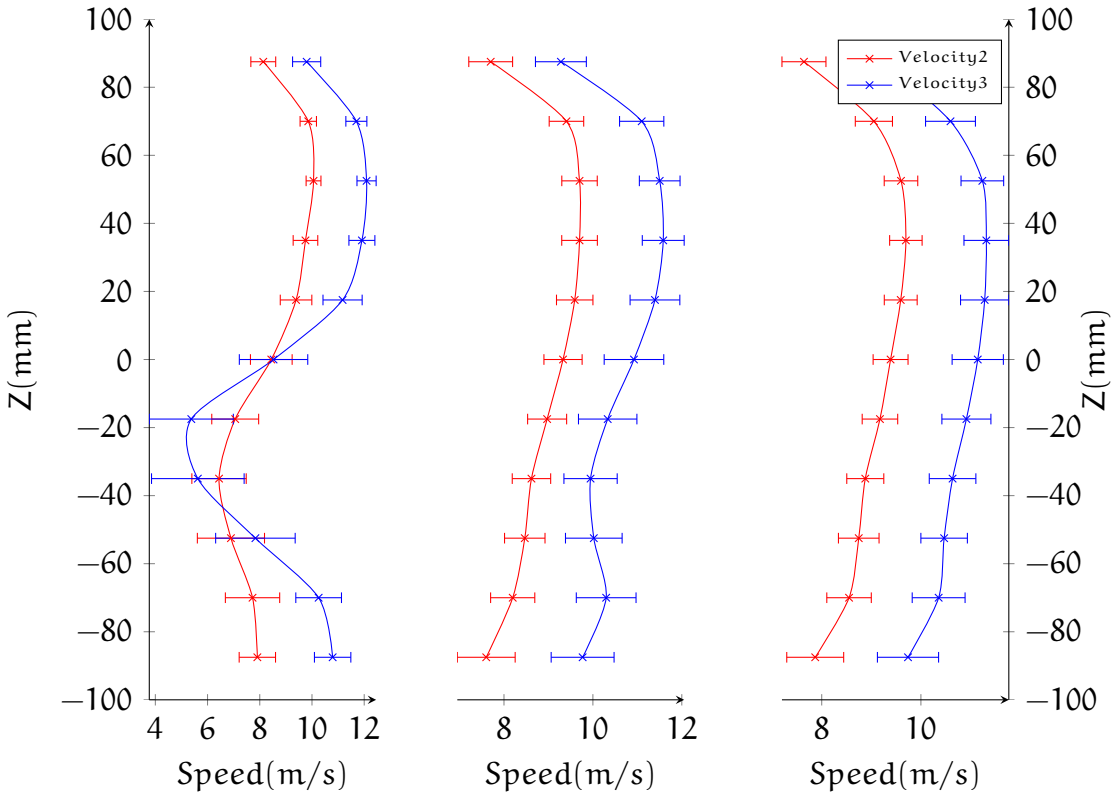

Figure 56: Section 5 Figure 57: Section 6 Figure 58: Section 7

Figure 59: FSI reinforced curves, Vertical (Y=0) (see Section 5.2.2 for information about section positioning)

Tables

Each table contains the speed and the associated error for each measurement point and fan-velocity.

Table 23: FSI NON reinforced Section 5

$Z(mm)$	$V_2(m/s)$	$e_2(m/s)$	$V_3(m/s)$	$e_3(m/s)$
−87,5	7,907	0,696	10,791	0,697
−70,0	7,723	1,040	10,255	0,875
−52,5	6,896	1,286	7,833	1,523
−35,0	6,440	1,041	5,628	1,773
−17,5	7,059	0,898	5,378	1,610
0,0	8,441	0,799	8,528	1,310
17,5	9,390	0,604	11,172	0,750
35,0	9,750	0,471	11,912	0,497
52,5	10,059	0,284	12,090	0,367
70,0	9,858	0,314	11,700	0,402
87,5	8,134	0,476	9,796	0,539

Table 24: FSI NON reinforced Section 6

$Z(mm)$	$V_2(m/s)$	$e_2(m/s)$	$V_3(m/s)$	$e_3(m/s)$
−87,5	7,601	0,651	9,769	0,708
−70,0	8,196	0,497	10,299	0,672
−52,5	8,468	0,455	10,021	0,637
−35,0	8,618	0,432	9,948	0,599
−17,5	8,971	0,439	10,333	0,657
0,0	9,328	0,429	10,924	0,670
17,5	9,591	0,410	11,396	0,560
35,0	9,700	0,401	11,582	0,471
52,5	9,699	0,399	11,503	0,458
70,0	9,405	0,388	11,098	0,498
87,5	7,701	0,493	9,280	0,572

Table 25: FSI NON reinforced Section 7

Z(mm)	$V_2(m/s)$	$e_2(m/s)$	$V_3(m/s)$	$e_3(m/s)$
−87,5	7,869	0,574	9,740	0,617
−70,0	8,551	0,449	10,358	0,533
−52,5	8,747	0,409	10,468	0,469
−35,0	8,878	0,373	10,638	0,470
−17,5	9,174	0,358	10,917	0,494
0,0	9,388	0,352	11,146	0,517
17,5	9,593	0,332	11,286	0,487
35,0	9,697	0,327	11,319	0,451
52,5	9,598	0,338	11,239	0,430
70,0	9,052	0,375	10,597	0,503
87,5	7,642	0,444	9,221	0,539

6.3.3 *High-speed Analysis,NON reinforced*

The following graphics show the dynamics of the standard flexible part (#2 see Figure 19) itself. Steady state and transitional recordings were taken. All measurements were done with V_2 and V_3. With high speed [Figure 60] the frequency is 8.33Hz in Y-direction and with low speed][Figure 62] the overall frequency is 3.33 Hz. Observing the movement of Figure 62 each oscillation has a complex movement in it.
The transitional measurements showing the time depend evolution to the stationary system. The complete development to the stationary system take 0.85s for Figure 64 and 0.7s for Figure 66.
The graphics show the movement of the 5 points in Z-and X'-direction in function of the time, every line represent one point. The trailing edge of the rigid plate is X'=0. The estimated measurement error for all points is 1.5mm.

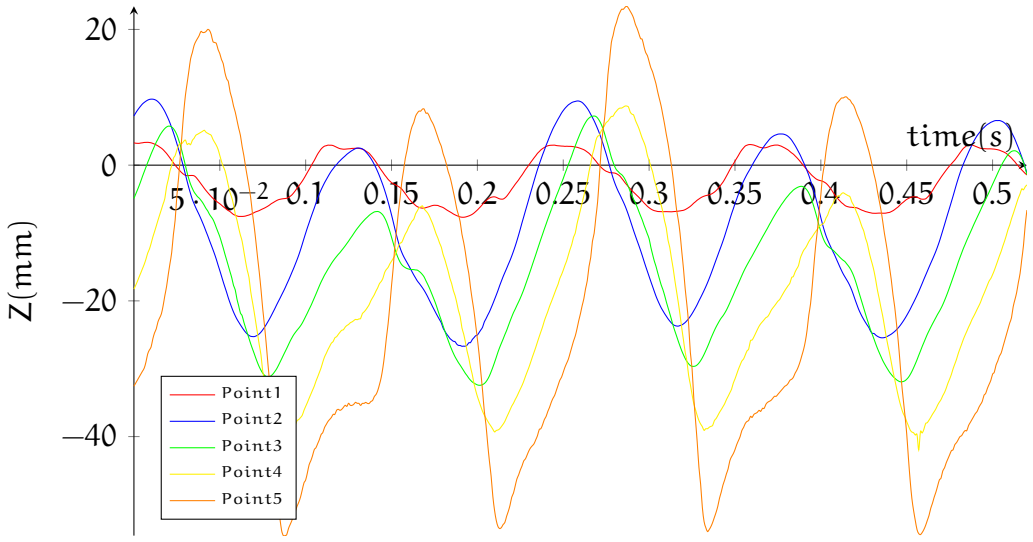

Figure 60: NON-reinforced flexible plate, V_3, steady state, Z-movement, (see Figure 5.2.2 for information about measurement point positioning)

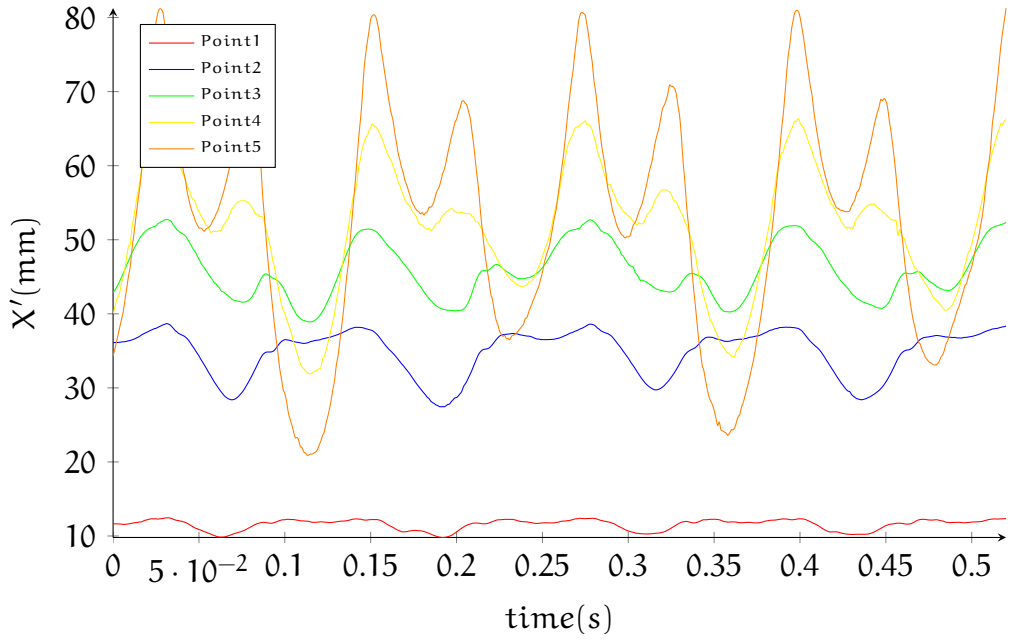

Figure 61: NON-reinforced flexible plate, V_3, steady state, X-movement, (see Figure 5.2.2 for information about measurement point positioning)

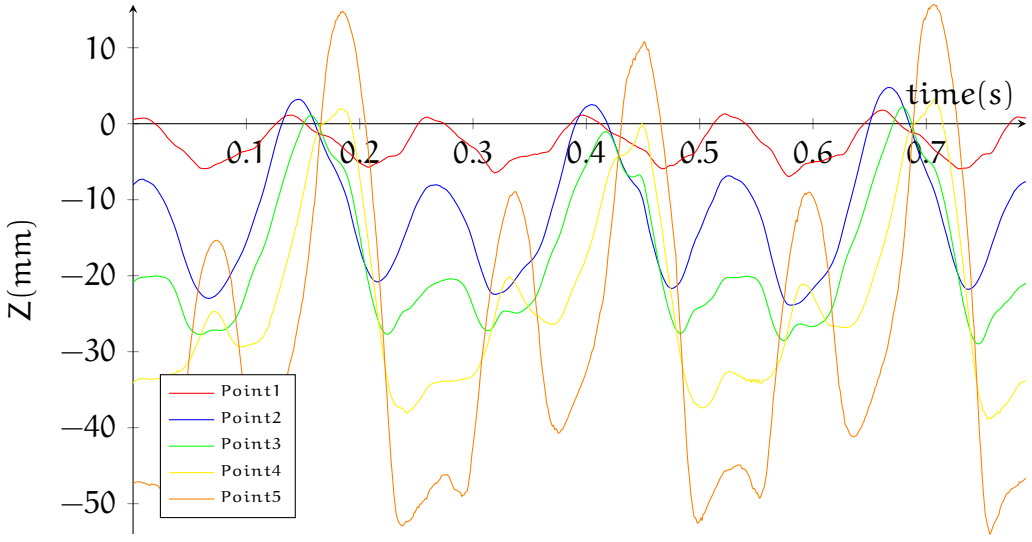

Figure 62: NON-reinforced flexible plate, V_2, steady state, Z-movement, (see Figure 5.2.2 for information about measurement point positioning)

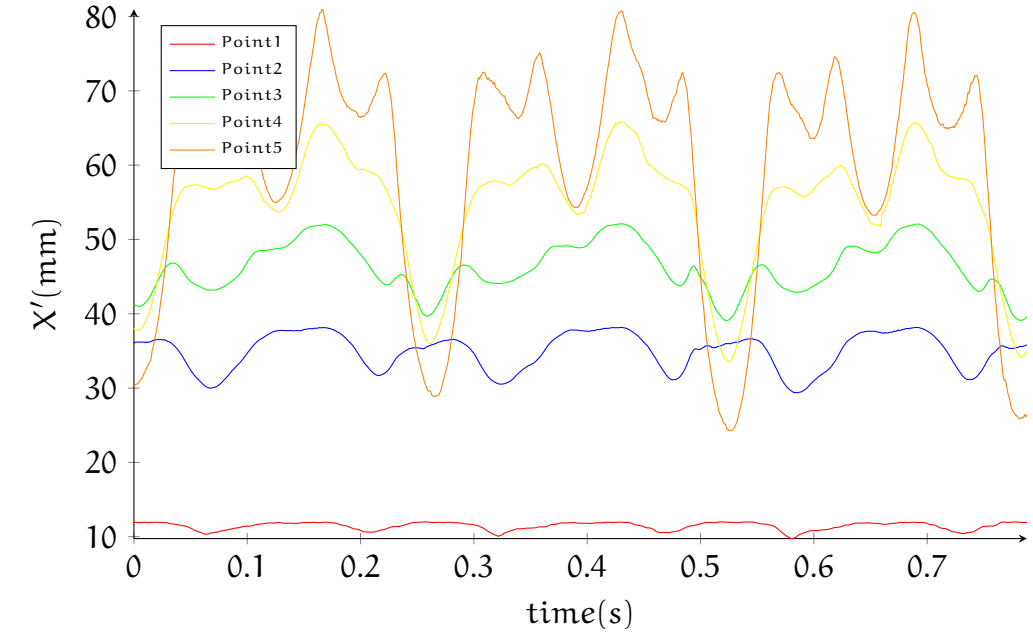

Figure 63: NON-reinforced flexible plate, V_3, steady state, X-movement, (see Figure 5.2.2 for information about measurement point positioning)

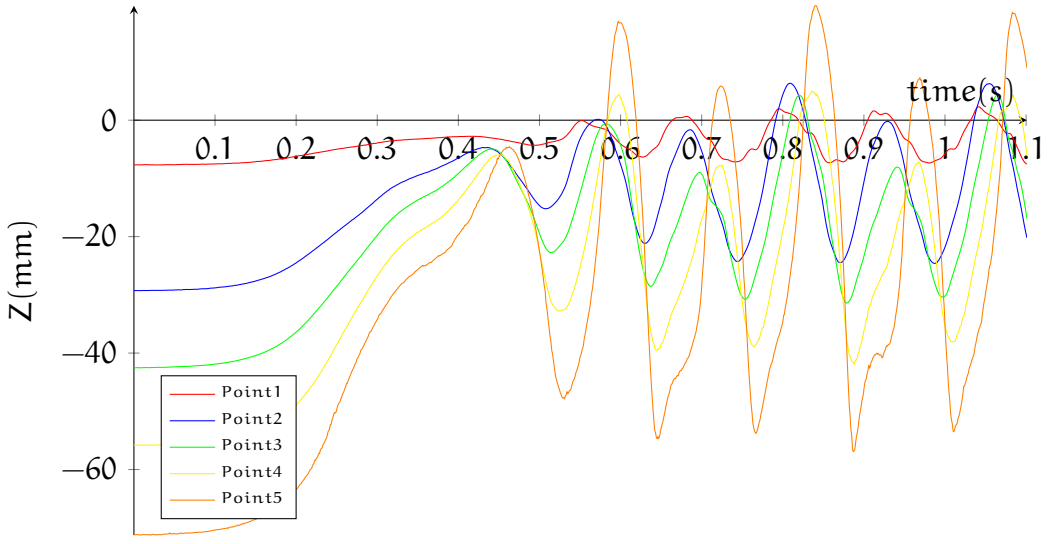

Figure 64: NON-reinforced flexible plate, V_3, transitional state, Z-movement, (see Figure 5.2.2 for information about measurement point positioning)

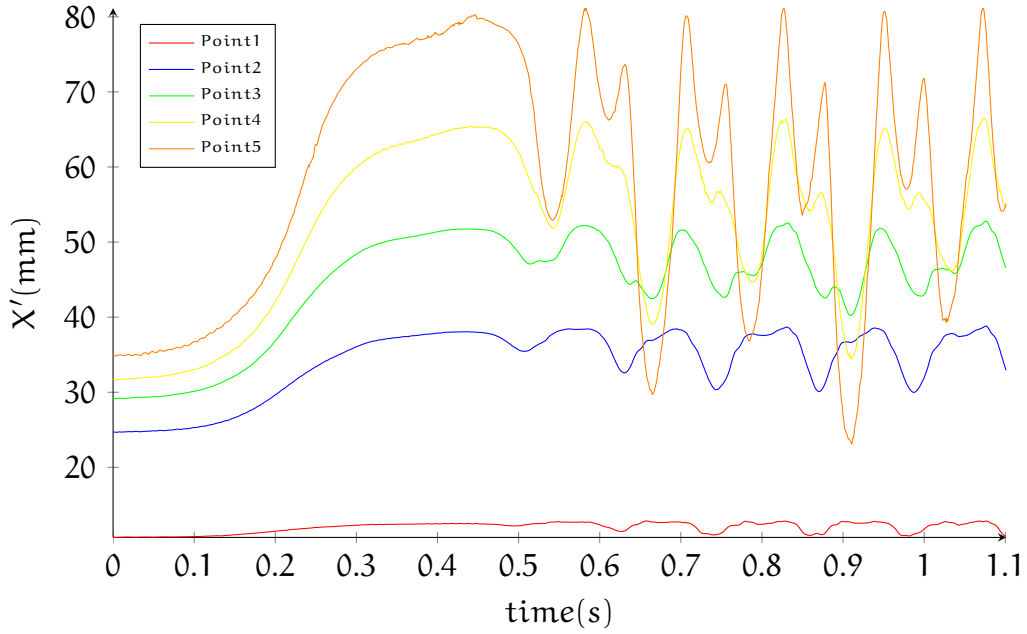

Figure 65: NON-reinforced flexible plate, V_3, steady state, X-movement, (see Figure 5.2.2 for information about measurement point positioning)

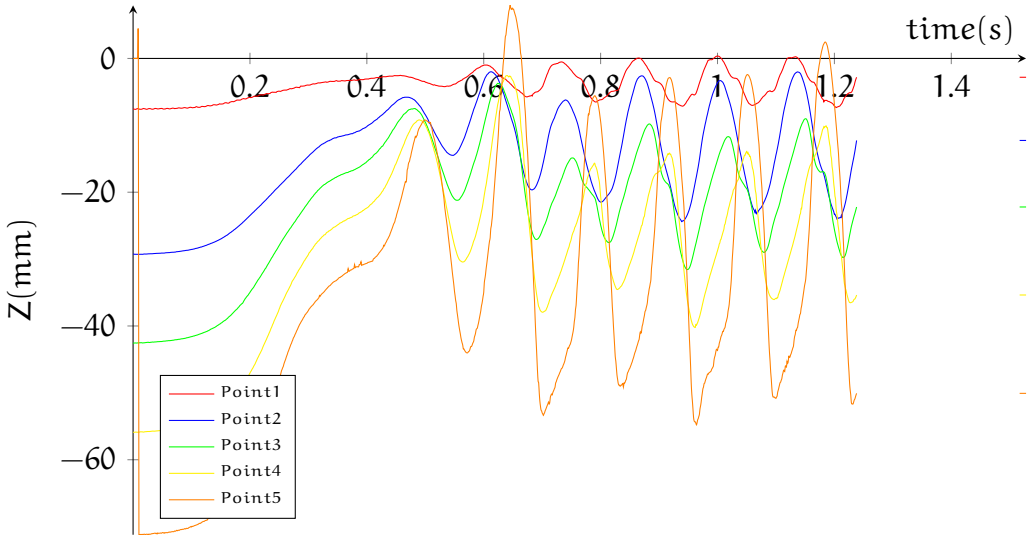

Figure 66: NON-reinforced flexible plate, V_2, transitional state, Z-movement, (see Figure 5.2.2 for information about measurement point positioning)

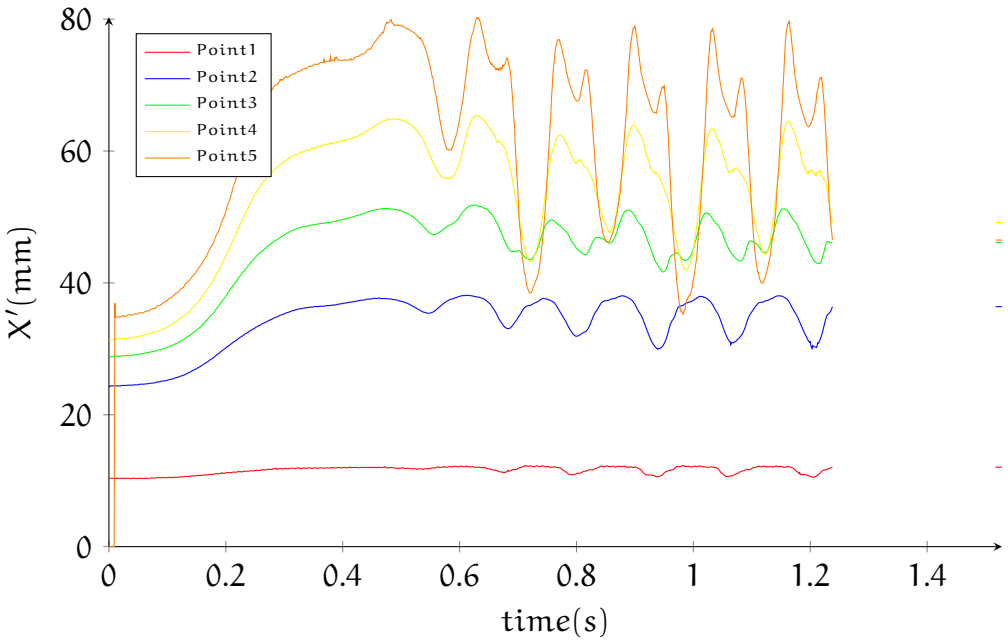

Figure 67: NON-reinforced flexible plate, V_2, transitional state, X-movement, (see Figure 5.2.2 for information about measurement point positioning)

6.3.4 *High-speed Analysis,reinforced*

The following graphics show the dynamics of the reinforced flexible part (#4 see Figure 19) itself. Steady state and transitional state recordings were taken. All measurements were done with V_2 and V_3. With V_3 [Figure 68] the frequency is 6.67Hz in Y-direction and with V_3[Figure 70] the overall frequency is 4 Hz. Observing the movement of Figure 70 each oscillation has a complex movement in it.
The transitional measurements showing the time depend evolution of the steady state system. The complete development to the stationary system takes 0.8s for Figure 72 and 1.05s for Figure 74. The graphics show the movement of the 5 points in Z-and X'-direction in function of the time, every line represent one point. The trailing edge of the rigid plate is X'=0. The estimated measurement error for all points is 1.5mm. Comparing Figure 70 and Figure 62 it is clear that the movement of the flexible plate with reinforcement is much more stable than without reinforcement.

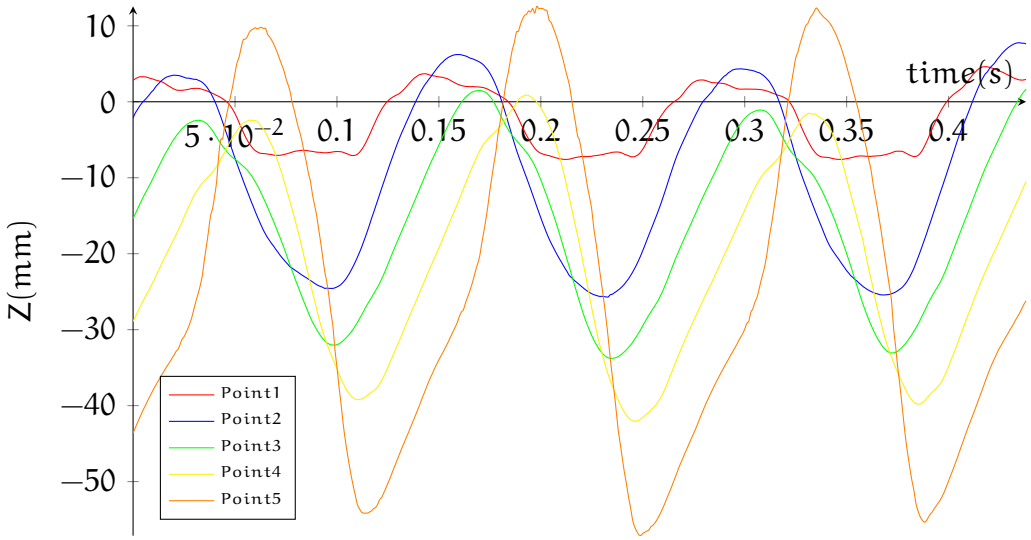

Figure 68: Reinforced flexible plate, V_3, steady state, Z-movement, (see Figure 5.2.2 for information about measurement point positioning)

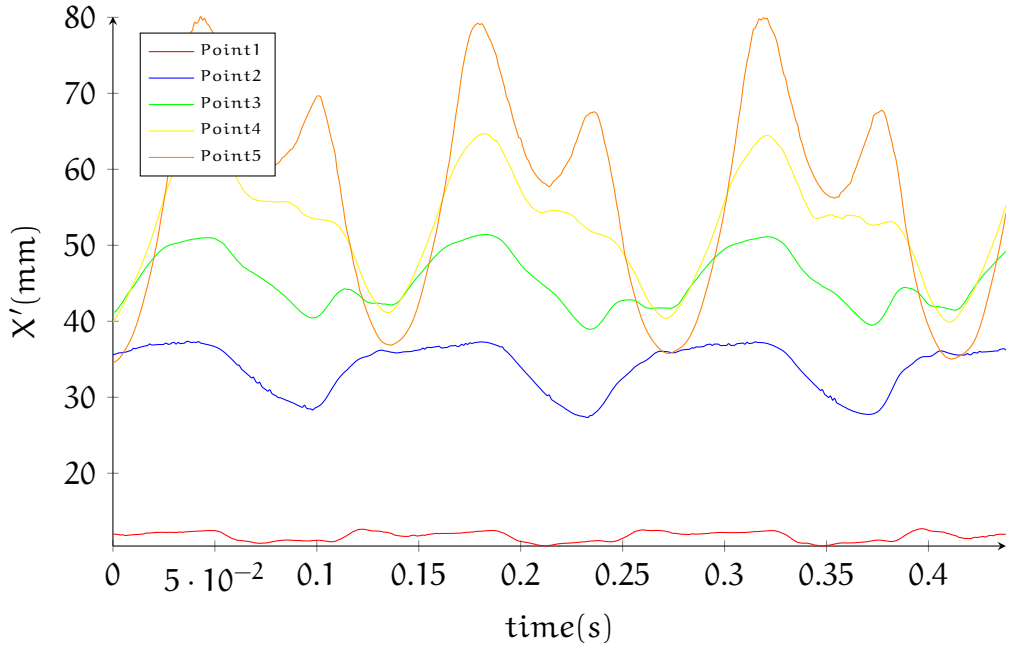

Figure 69: Reinforced flexible plate, V_3, steady state, X-movement, (see Figure 5.2.2 for information about measurement point positioning)

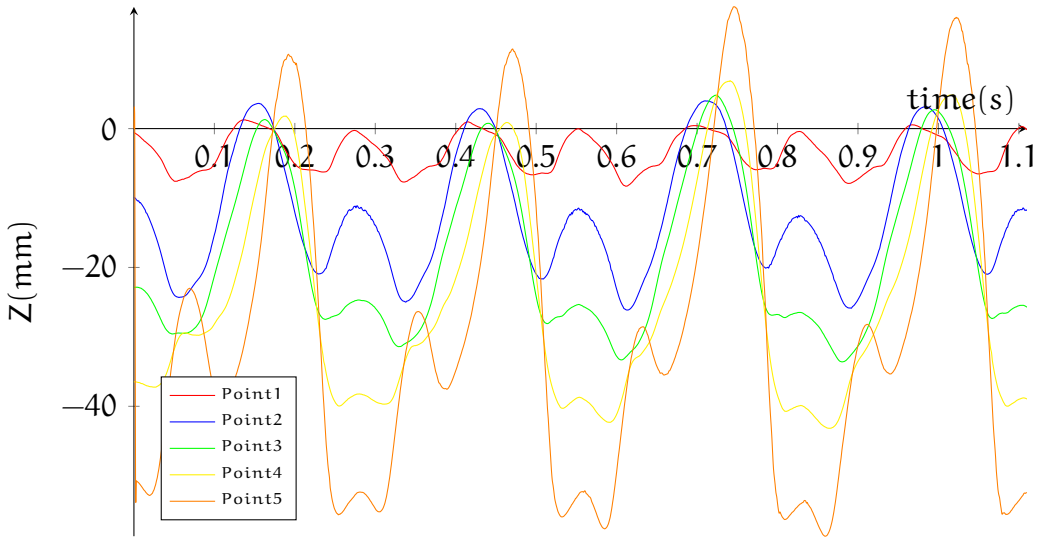

Figure 70: Reinforced flexible plate, V_2, steady state, Z-movement, (see Figure 5.2.2 for information about measurement point positioning)

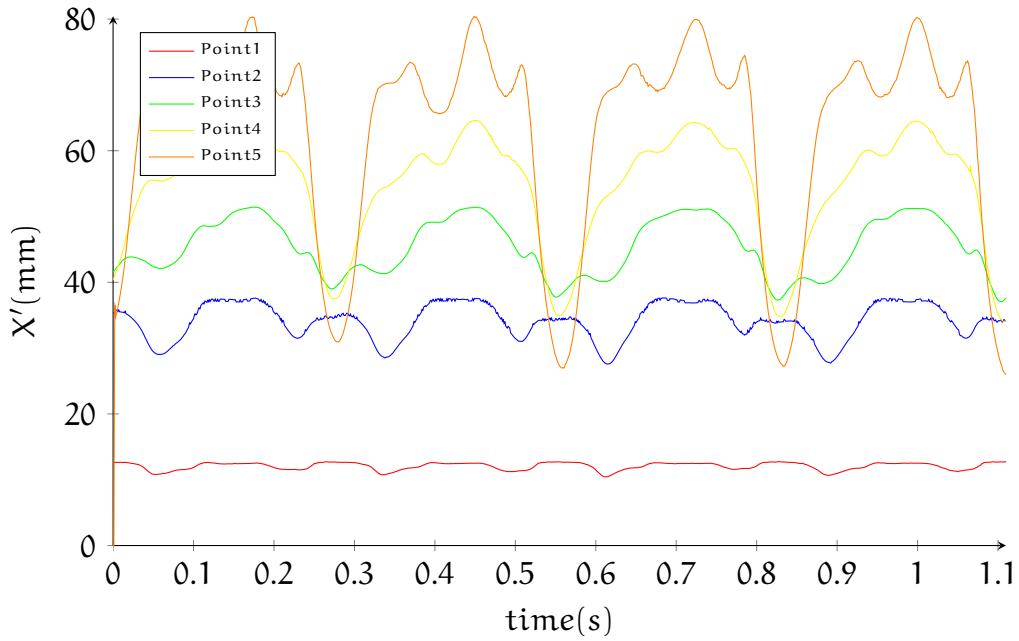

Figure 71: Reinforced flexible plate, V_2, steady state, X-movement, (see Figure 5.2.2 for information about measurement point positioning)

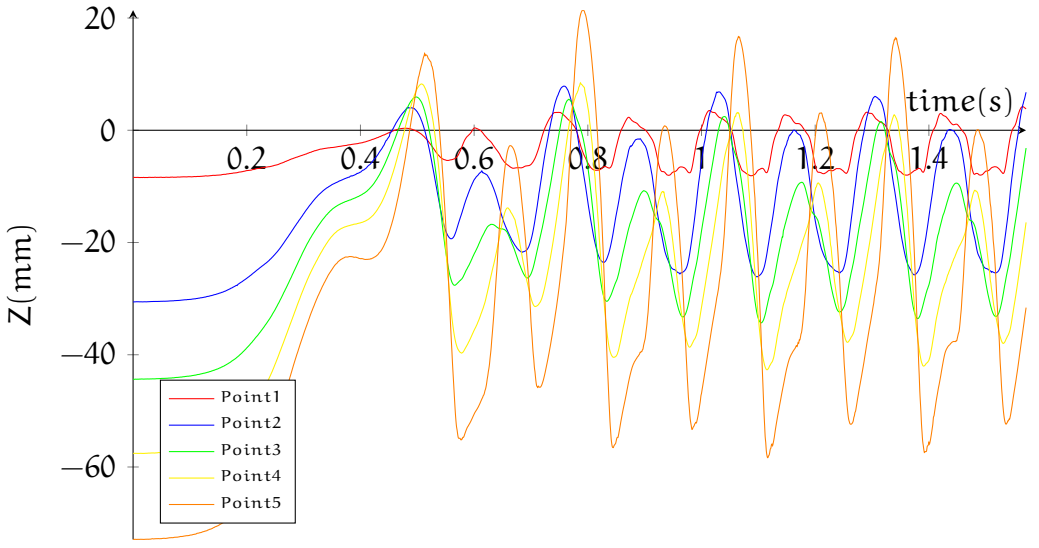

Figure 72: Reinforced flexible plate, V_3, transitional state, Z-movement, (see Figure 5.2.2 for information about measurement point positioning)

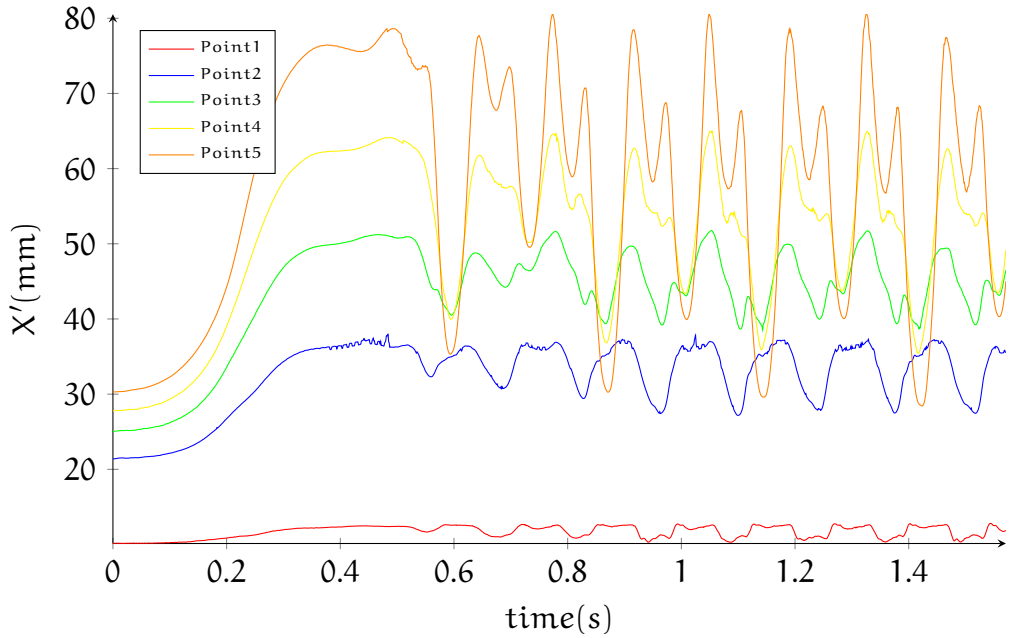

Figure 73: Reinforced flexible plate, V_3, transitional state, X-movement, (see Figure 5.2.2 for information about measurement point positioning)

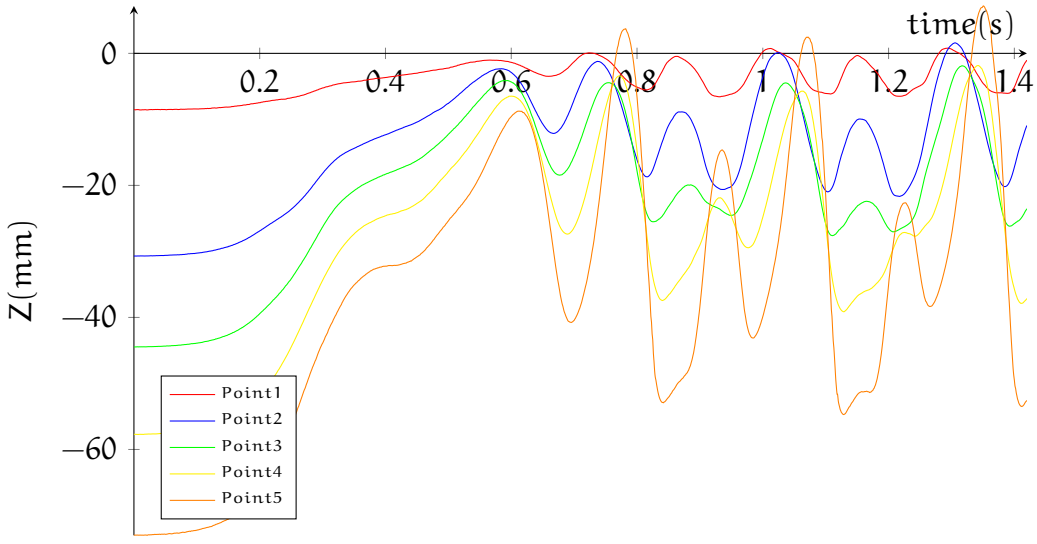

Figure 74: Reinforced flexible plate, V_2, transitional state, Z-movement, (see Figure 5.2.2 for information about measurement point positioning)

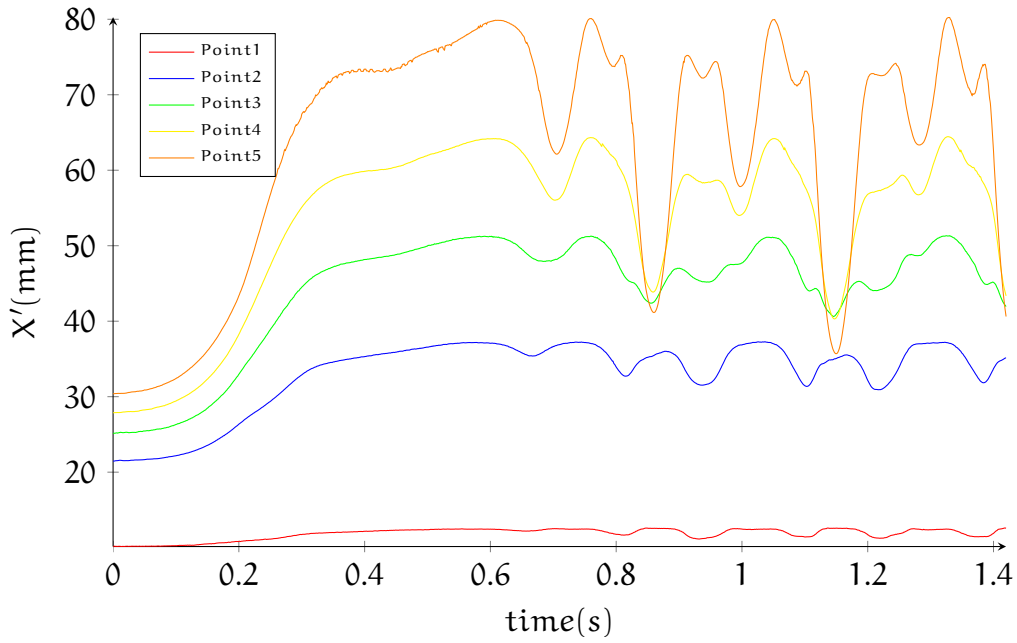

Figure 75: Reinforced flexible plate, V_2, transitional state, X-movement, (see Figure 5.2.2 for information about measurement point positioning)

6.4 CFD

The following graphic compares the dynamics of the CFD and the dynamics of the experiment. Only one point will be compared. Point5 in Y direction of the the reinforced, high-speed (V_2), steady state measurement compared with the trailing edge point of the CFD study. As we can observe the frequency does not coincide, also the movement and the distribution are slightly different. This is caused by different problems:

- First of all the input flow velocity of the experiment (U_e) and the CFD study (U_0) are not equal.

$$U_0 = 10m/s \tag{17}$$
$$U_e \approx 11m/s \tag{18}$$

- Not all necessary material characteristics for the simulation were available at the data sheet. Estimate values from similar silicone's were used.
- The gravity force affects the flexible plate in reality much more than in the simulation (down force equal to the silicone weight was programmed), easy to see as the flexible part sags much more in the experiment than in the simulation.
- The geometry of the rigid plate is different in the cfd study (rectangular plate) than in the experiment (full-symmetrical airfoil).

Taking all these facts in account a qualitative approximation was obtained.

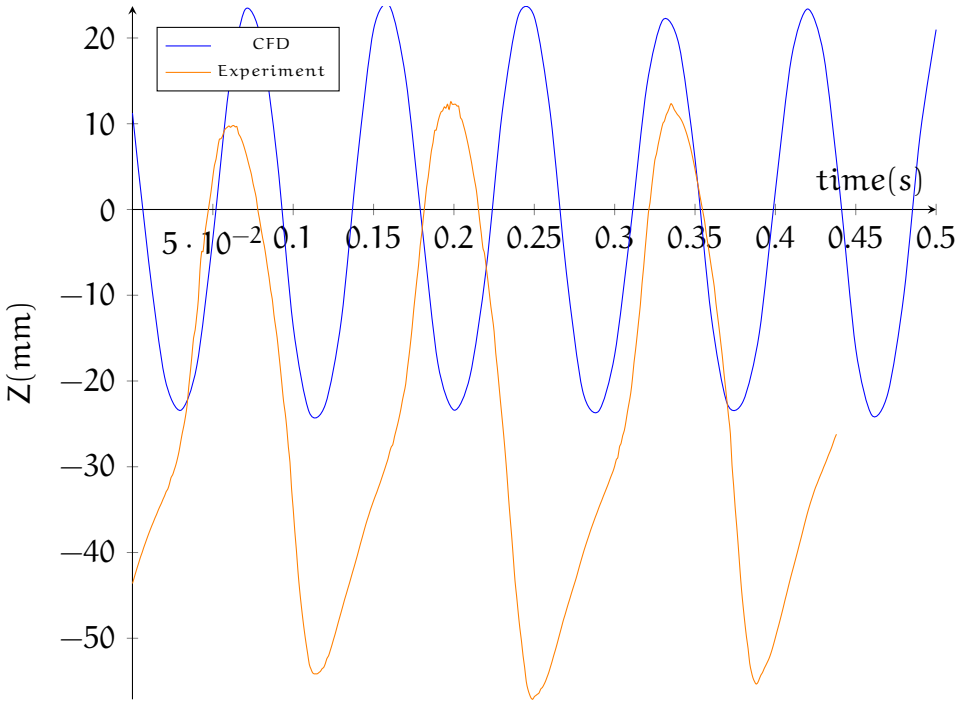

Figure 76: Comparison CFD with experiment, stationary Point 5

7

CONCLUSION AND OUTLOOK

7.1 CONCLUSION

The main interest of thesis was to design and fabricate an experimental method to validate a CFD code for FSI which will be used for the treatment of OSAS.

From the design view a simplified structure of the human respiratory system was realized and planned. After studying different possibilities, silicon was used to fabricate the flexible part, which corresponds to the pharynx. Some reinforcements were plugged into some of the flexible plates to increase the transverse stability what would help to obtain 2-D results. The fixed plate corresponds to the fixed structures in the human airways. Different models were produced with Computer numerical controlled machines (CNC) until a perfect symmetrical part was obtained to guarantee reliable experimental results.

The project was difficult to realize due to its short time frame, however high quality results (see Section 6.4) could be obtained. Observing the results a uniform and homogeneous inlet-flow was created, the error in all measurements (see tables in Chapter 6) are minimal. Thus, the experimental data can be used for the validation of CFD tools. Boundary Layer measurements confirmed a laminar flow in the testrig [Section 6.2.2]. Thanks to the similarity of the rigid plate to an airfoil the boundary layers are really thin increasing the Fluid Structure Interaction between the air and the flexible silicone plate, simplifying also the CFD calculations. Flow measurements over all sections showed perfect symmetry lateral and vertical to the rigid plate. FSI measurements taken with pitot tubes showed interesting behavior (strong decrease of velocity in the oscillation area of the flexible plate [Figure 55]) at average values. As expected a strong decrease of the velocity in the "oscillating zone" appeared. Due to the turbulent flow in FSI measurements, static pressure was taken outside the testrig, even so, due to the vortices (effect of the proper movement) in the area behind the flapping part, the airflow-vector had some Z-components, what produced a

variation in the pitot-tube measurements (just X-axis flow can be measured) and this produced high errors where the flexible part moved. The highspeed recordings reveled the dynamics of the FSI. For the different silicone plates strong differences in dynamics appeared. The non reinforced flag has a much more complicated cycle, than the reinforced one. All recordings with the different velocities and materials showed a repetitive cycling over the time [7, 6], confirming our high quality results. This master thesis can be concluded, with the satisfaction of having managed to bring the theoretical studies a little closer to reality, and thus to get with all participants of this research, a little bit closer to a treatment for OSAS, that provides quality and better life expectancy to those affected by this diagnosis.

7.2 OUTLOOK

Despite the fact that satisfactory results were obtained, the use of pitot tube has the inconvenient that just average values could be obtained. For more detailed flow information the use of hotwires is of need. Even if no such experimentation were done, the testrig was constructed to change the inclination angle of the cube. This would be useful to take more measurements simulating the inclination of a human being. Another possibility of the testrig is to change the position of the rigid plate from horizontal to vertical. Putting the rigid plate vertically in the cube or using a material with lower density for the flexible part would possibly eliminate or at least reduce the effect of gravity.Another possible experiment is to obstruct one of the inlet areas to simulate a partial obstruction of the human airways. The use of a different material with lower density for the flapping part would allow to decrease the inflow velocity, what would increase the similarity to the human breathing. All these improvement can be realized using the actual testrig without any changes, if therefore is any need.

Part IV

APPENDIX

APPENDIX

A.1 TECHNICAL DRAWINGS

In this sections are all plans used for the construction listed.

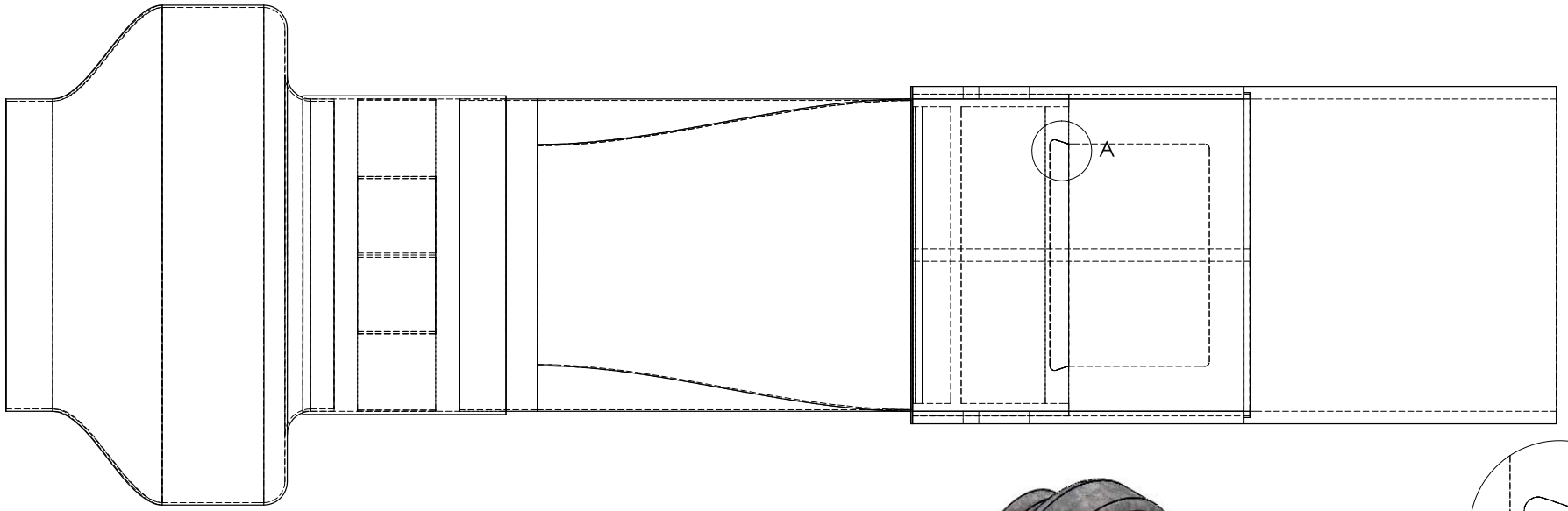

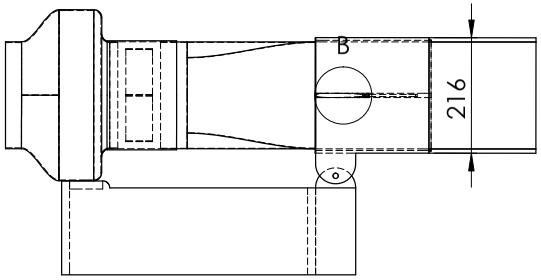

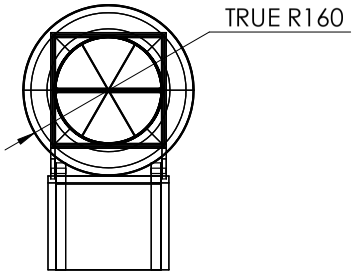

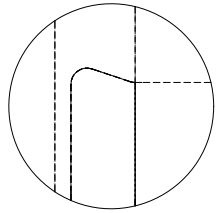

DETAIL A
MAßSTAB 1 : 1

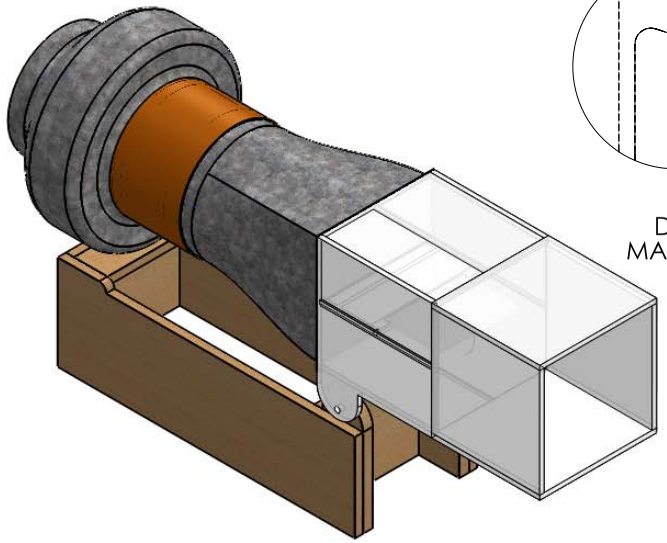

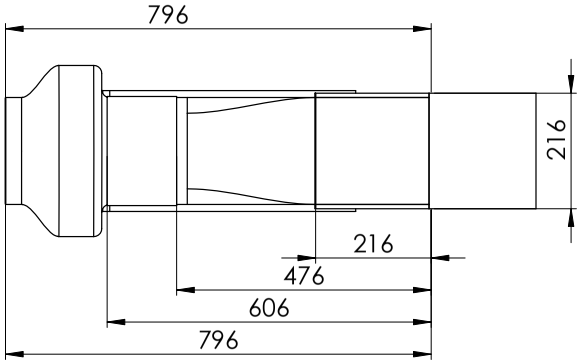

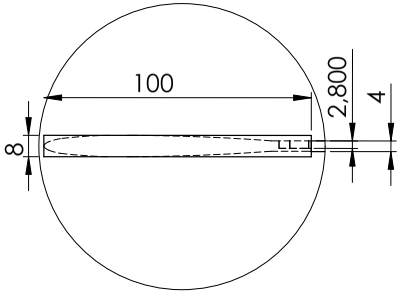

DETAIL B
MAßSTAB 1 : 2

UNLESS OTHERWISE SPECIFIED: DIMENSIONS ARE IN MILLIMETERS SURFACE FINISH: TOLERANCES: LINEAR: ANGULAR:		FINISH:		DEBUR AND BREAK SHARP EDGES	DO NOT SCALE DRAWING	REVISION
	NAME	SIGNATURE	DATE		TITLE:	
DRAWN						
CHK'D						
APPV'D						
MFG						
Q.A				MATERIAL:	DWG NO. MAIN_DESIGN_PLAN_1	A3
				WEIGHT:	SCALE:1:5	SHEET 1 OF 2

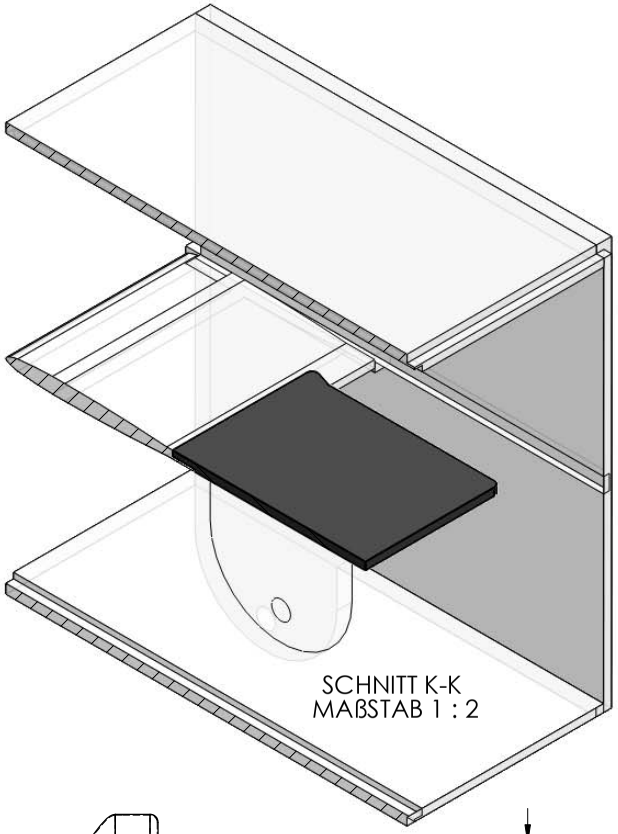

SCHNITT K-K
MAßSTAB 1 : 2

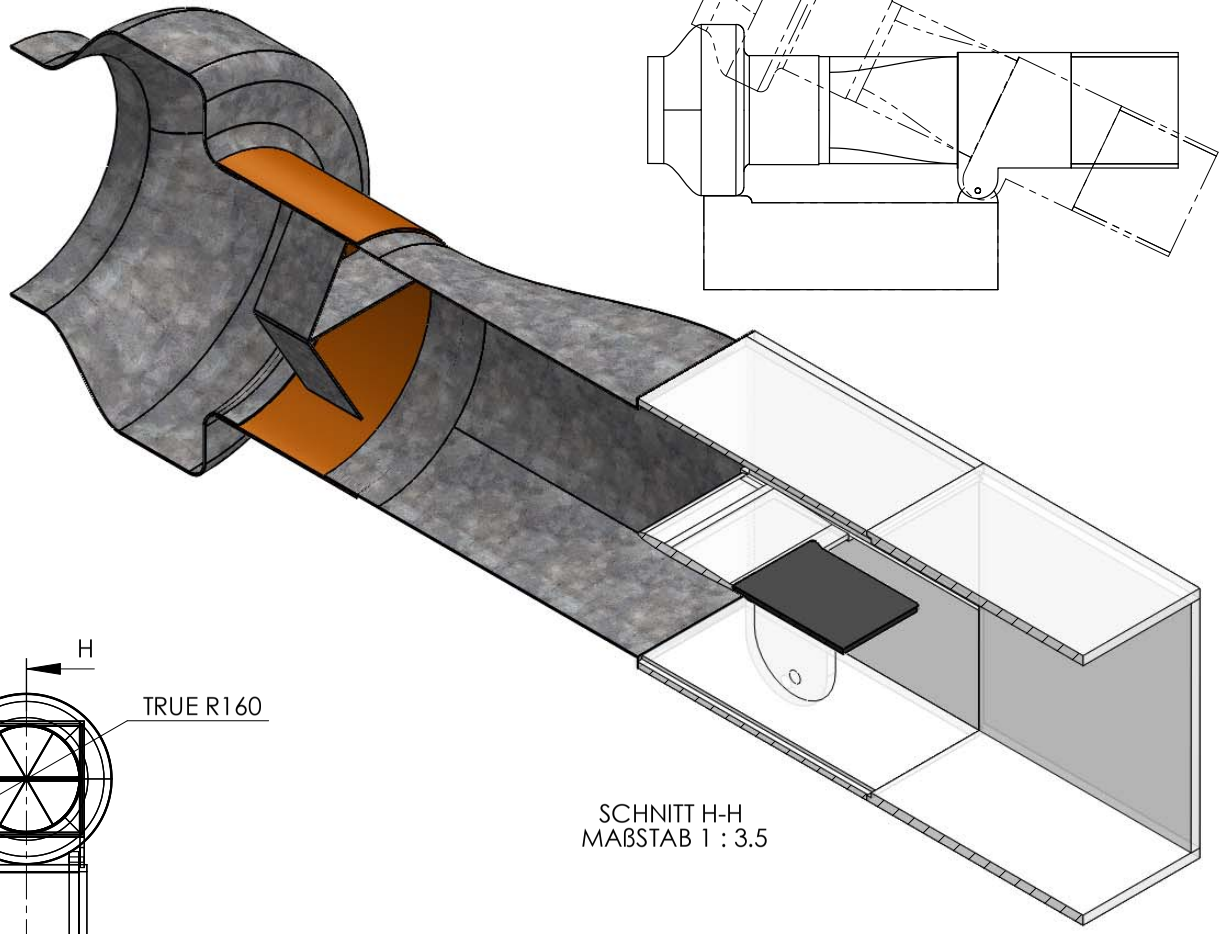

SCHNITT H-H
MAßSTAB 1 : 3.5

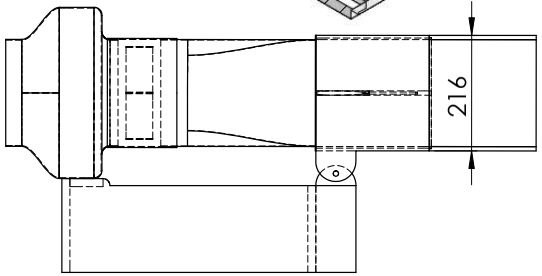

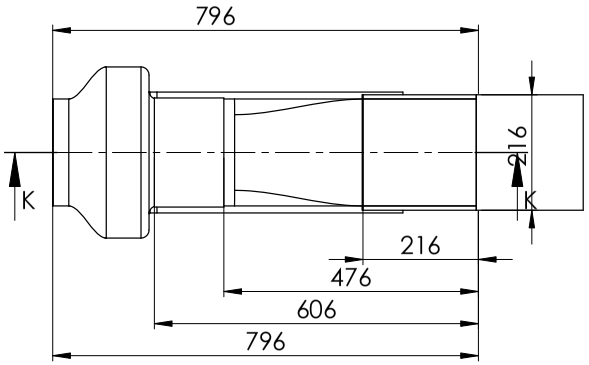

UNLESS OTHERWISE SPECIFIED: DIMENSIONS ARE IN MILLIMETERS SURFACE FINISH: TOLERANCES: LINEAR: ANGULAR:		FINISH:		DEBUR AND BREAK SHARP EDGES		DO NOT SCALE DRAWING	REVISION
	NAME	SIGNATURE	DATE			TITLE:	
DRAWN							
CHK'D							
APPV'D							
MFG							
Q.A				MATERIAL:		DWG NO. MAIN_DESIGN_PLAN_1	A3
				WEIGHT:		SCALE:1:5	SHEET 2 OF 2

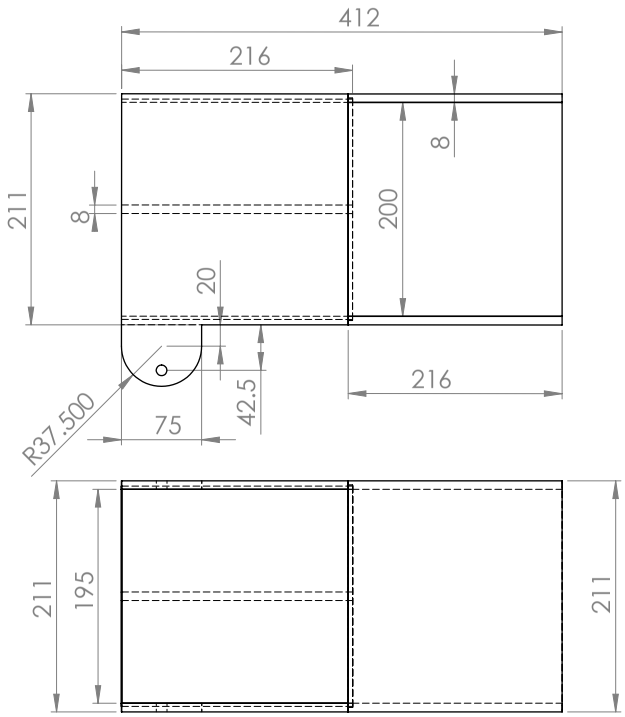

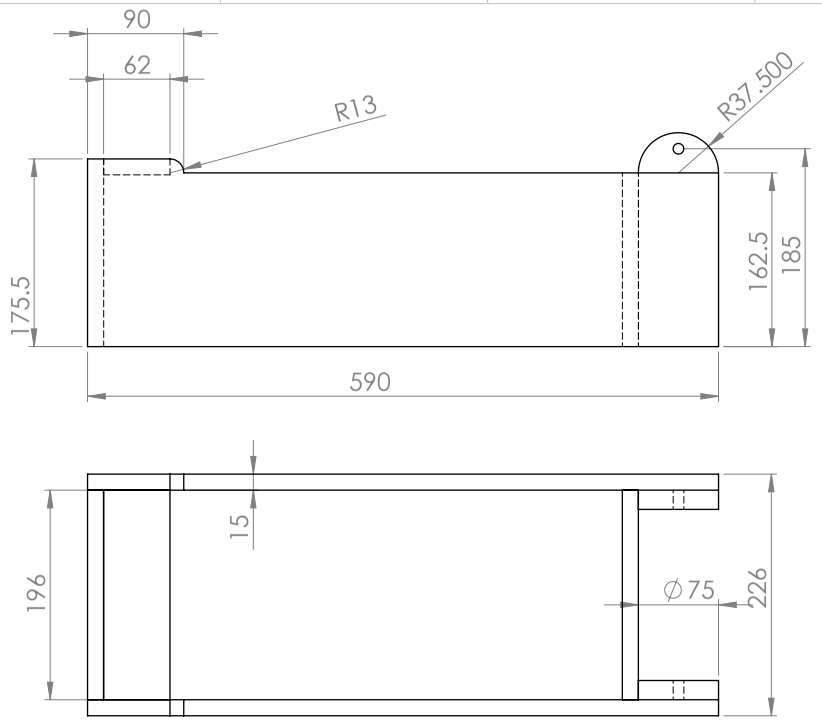

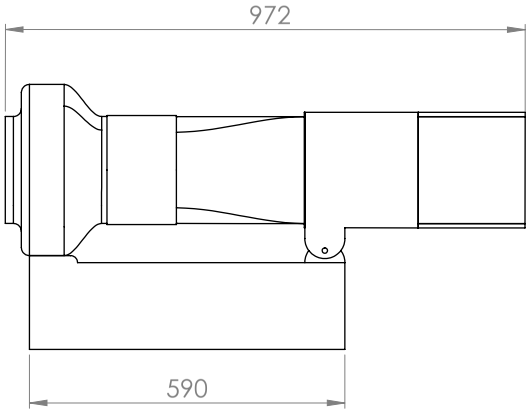

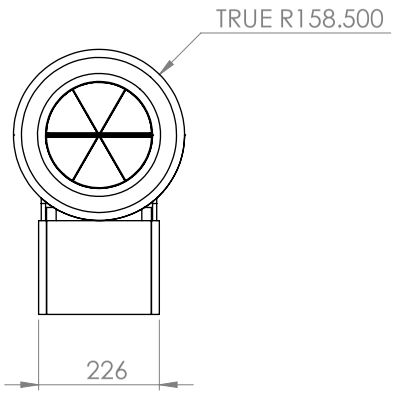

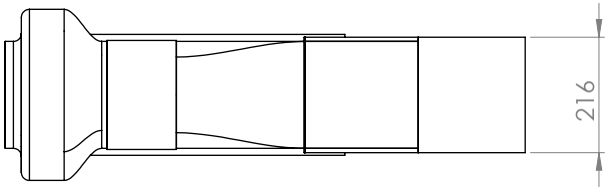

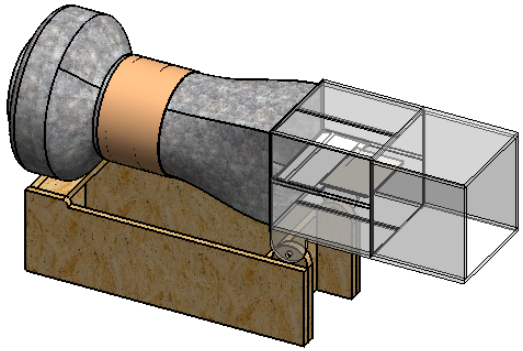

UNLESS OTHERWISE SPECIFIED: DIMENSIONS ARE IN MILLIMETERS SURFACE FINISH: TOLERANCES: LINEAR: ANGULAR:		FINISH:		DEBUR AND BREAK SHARP EDGES	DO NOT SCALE DRAWING	REVISION
	NAME	SIGNATURE	DATE		TITLE:	
DRAWN						
CHK'D						
APPV'D						
MFG						
Q.A				MATERIAL:	DWG NO.	A3
				WEIGHT:	SCALE:1:10	SHEET 1 OF 1

MAIN_DESIGN_PLAN_2

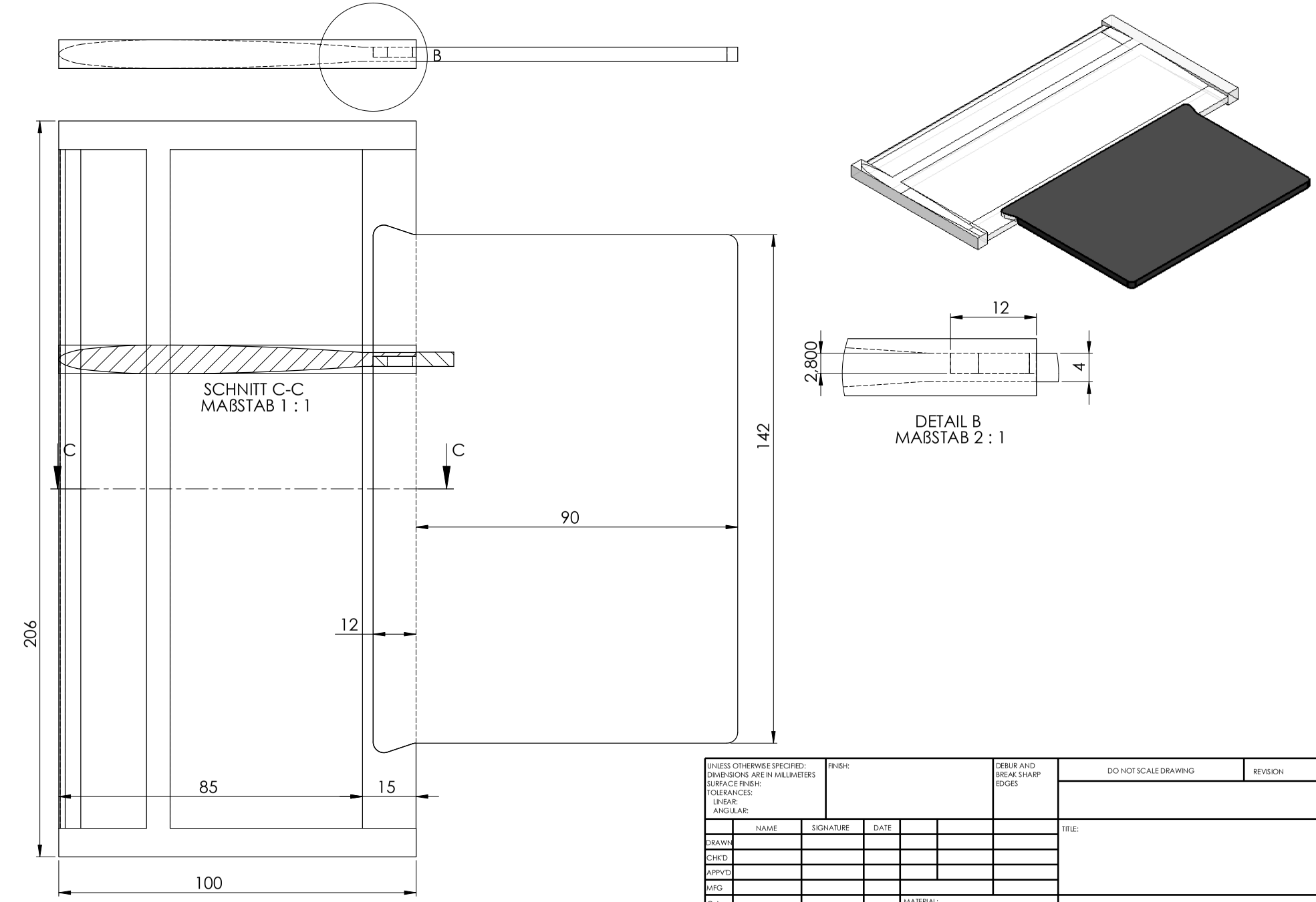

UNLESS OTHERWISE SPECIFIED: DIMENSIONS ARE IN MILLIMETERS SURFACE FINISH: TOLERANCES: LINEAR: ANGULAR:		FINISH:		DEBUR AND BREAK SHARP EDGES		DO NOT SCALE DRAWING	REVISION
	NAME	SIGNATURE	DATE			TITLE:	
DRAWN							
CHK'D							
APPV'D							
MFG							
Q.A				MATERIAL:		DWG NO. INNER_PARTS	A3
				WEIGHT:		SCALE:1:2	SHEET 1 OF 1

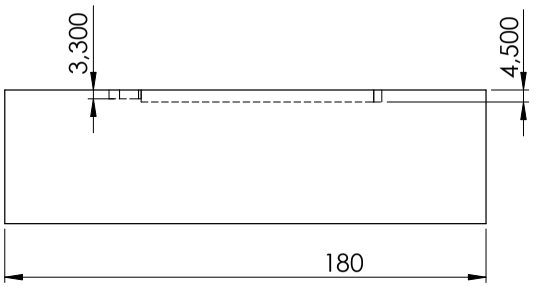

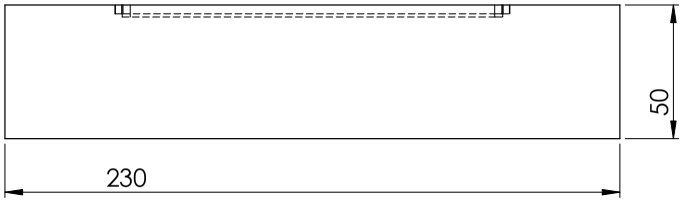

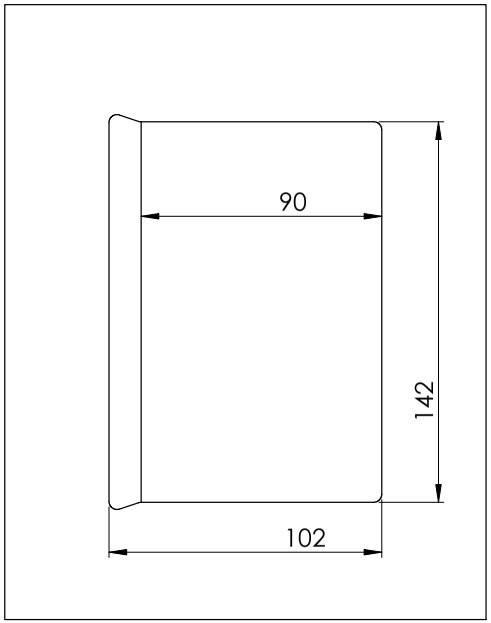

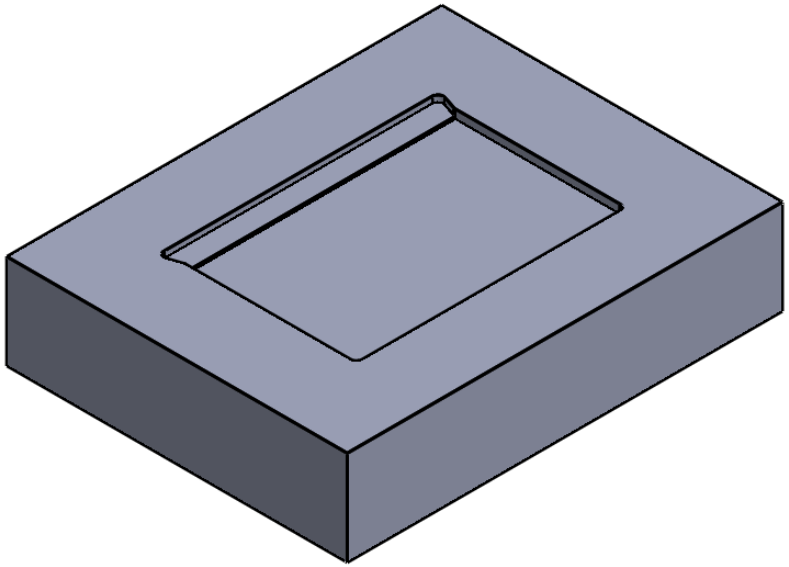

UNLESS OTHERWISE SPECIFIED: DIMENSIONS ARE IN MILLIMETERS SURFACE FINISH: TOLERANCES: LINEAR: ANGULAR:	FINISH:		DEBUR AND BREAK SHARP EDGES	DO NOT SCALE DRAWING	REVISION		
	NAME	SIGNATURE	DATE				TITLE:
DRAWN							
CHK'D							
APPV'D							
MFG							
Q.A				MATERIAL:			DWG NO. NEGATIV_FORM
							A3
				WEIGHT:		SCALE:1:2	SHEET 1 OF 1

A.6 PRESSURE TABLES

A.6.1 *Calibration*

Table 26: Calibration Section 1 Horizontal, pressure

Y(mm)	P_1(m/s)	e_1(m/s)	P_2(m/s)	e_2(m/s)	P_3(m/s)	e_3(m/s)
−87,5	18,232	2,194	32,170	3,639	49,751	4,527
−70,0	23,436	1,631	41,919	2,478	62,615	3,307
−52,5	25,284	1,451	45,990	2,151	68,227	2,679
−35,0	26,806	1,364	48,556	2,009	71,010	2,399
−17,5	27,694	1,280	48,695	1,829	72,580	2,160
0,0	28,354	1,256	47,566	1,942	72,529	2,324
17,5	28,633	1,311	45,669	2,019	71,204	2,587
35,0	27,819	1,365	42,824	1,990	67,666	2,753
52,5	27,147	1,300	41,417	1,996	63,250	2,981
70,0	26,276	1,490	40,100	2,230	57,302	3,732
87,5	18,742	2,005	30,195	2,948	40,532	4,465

Table 27: Calibration Section 1 Vertical, pressure

Z(mm)	P_1(m/s)	e_1(m/s)	P_2(m/s)	e_2(m/s)	P_3(m/s)	e_3(m/s)
−87,5	17,935	2,146	29,129	3,174	42,178	4,195
−70,0	24,450	1,604	39,266	2,360	55,719	2,856
−52,5	26,963	1,546	42,875	2,171	60,098	3,026
−35,0	28,667	1,345	45,375	2,142	64,836	2,925
−17,5	29,363	1,263	47,573	1,997	68,920	2,608
0,0	29,382	1,240	48,381	1,844	70,754	2,276
17,5	28,161	1,295	47,848	1,871	69,303	2,475
35,0	26,838	1,375	46,344	1,948	66,747	2,647
52,5	25,628	1,506	44,229	2,270	63,324	2,931
70,0	23,974	1,731	41,703	2,539	60,004	3,314
87,5	18,426	2,434	30,752	3,310	46,272	4,558

Table 28: Calibration Section 2 Horizontal, pressure

Y(mm)	$P_1(m/s)$	$e_1(m/s)$	$P_2(m/s)$	$e_2(m/s)$	$P_3(m/s)$	$e_3(m/s)$
−87,5	16,181	1,911	29,011	2,841	41,936	3,615
−70,0	22,963	1,714	40,905	2,422	58,334	3,090
−52,5	25,468	1,268	44,823	2,039	63,941	2,442
−35,0	26,575	1,174	47,237	1,689	67,587	2,203
−17,5	28,148	0,987	48,441	1,412	69,166	2,004
0,0	28,346	0,924	48,107	1,473	69,168	1,849
17,5	27,368	1,038	46,601	1,734	67,300	2,004
35,0	26,143	1,108	44,311	2,015	64,897	2,248
52,5	24,322	1,187	41,506	2,195	61,531	2,862
70,0	22,523	1,561	37,205	2,600	57,400	3,292
87,5	17,532	2,017	26,603	3,153	42,342	4,107

Table 29: Calibration Section 2 Vertical, pressure

Z(mm)	$P_1(m/s)$	$e_1(m/s)$	$P_2(m/s)$	$e_2(m/s)$	$P_3(m/s)$	$e_3(m/s)$
−87,5	16,786	1,811	26,553	2,851	38,481	3,913
−70,0	23,529	1,505	37,412	2,194	52,943	3,333
−52,5	25,383	1,269	40,799	1,936	57,466	2,814
−35,0	27,261	1,219	43,347	1,852	61,972	2,756
−17,5	28,496	0,972	46,155	1,761	65,150	2,356
0,0	28,755	0,957	47,532	1,492	67,266	1,944
17,5	28,258	0,942	47,045	1,460	66,646	1,980
35,0	27,349	1,055	45,751	1,621	64,362	2,311
52,5	26,118	1,240	43,896	1,876	62,531	2,683
70,0	24,914	1,395	41,429	2,238	58,091	3,968
87,5	17,507	1,998	30,863	2,955	42,545	4,158

Table 30: Calibration Section 3 Horizontal, pressure

Y(mm)	$P_1(m/s)$	$e_1(m/s)$	$P_2(m/s)$	$e_2(m/s)$	$P_3(m/s)$	$e_3(m/s)$
−87,5	15,899	1,880	27,703	2,830	40,544	3,527
−70,0	22,813	1,797	38,427	2,712	55,573	3,267
−52,5	25,470	1,316	42,988	2,095	62,127	2,239
−35,0	26,842	0,998	45,279	1,622	65,382	2,137
−17,5	27,898	0,853	46,669	1,371	66,935	1,820
0,0	28,025	0,816	47,108	1,383	66,788	1,895
17,5	27,078	0,987	45,719	1,568	65,338	2,041
35,0	25,818	1,046	44,149	1,671	63,388	2,233
52,5	23,856	1,251	40,875	2,093	60,630	2,774
70,0	21,475	1,762	36,687	2,725	54,947	3,771
87,5	15,263	1,917	25,572	2,869	44,703	4,390

Table 31: Calibration Section 3 Vertical, pressure

Z(mm)	$P_1(m/s)$	$e_1(m/s)$	$P_2(m/s)$	$e_2(m/s)$	$P_3(m/s)$	$e_3(m/s)$
−87,5	14,247	1,613	23,227	2,640	33,317	3,644
−70,0	22,445	1,682	34,633	2,692	48,711	4,060
−52,5	25,232	1,127	38,844	1,830	55,304	2,765
−35,0	26,656	1,041	42,113	1,811	59,239	2,735
−17,5	27,771	0,944	44,603	1,660	62,847	2,348
0,0	28,061	0,851	46,087	1,390	65,563	1,897
17,5	27,716	0,803	45,982	1,242	65,444	1,840
35,0	27,057	0,971	45,175	1,467	64,012	2,096
52,5	26,024	1,107	43,110	1,878	61,109	2,754
70,0	24,500	1,421	40,369	2,642	57,511	3,667
87,5	17,953	1,862	31,172	2,974	44,138	4,177

A.6.2 *Flow measurement*

Table 32: Flow Section 1, pressure

Z(mm)	$P_1(m/s)$	$e_1(m/s)$	$P_2(m/s)$	$e_2(m/s)$	$P_3(m/s)$	$e_3(m/s)$
−87,5	21,088	2,151	32,722	3,201	54,592	4,197
−70,0	29,569	1,639	45,220	2,403	70,483	3,133
−52,5	31,506	1,533	49,486	2,612	75,817	3,256
−35,0	33,348	1,354	52,855	2,412	80,567	3,311
−17,5	33,753	1,362	56,074	2,217	85,108	3,086
0,0	0,000	0,000	0,000	0,000	0,000	0,000
17,5	30,010	1,442	52,088	2,234	79,714	2,380
35,0	28,168	1,443	50,873	2,148	77,700	2,297
52,5	26,473	1,477	50,065	2,135	74,581	2,657
70,0	26,092	1,621	49,177	2,239	70,280	2,859
87,5	20,912	2,470	36,126	3,292	59,326	3,995

Table 33: Flow Section 2, pressure

Z(mm)	$P_1(m/s)$	$e_1(m/s)$	$P_2(m/s)$	$e_2(m/s)$	$P_3(m/s)$	$e_3(m/s)$
−87,5	22,811	2,247	36,021	3,143	59,284	3,932
−70,0	28,944	1,616	44,135	2,280	69,403	2,721
−52,5	30,576	1,346	46,592	2,390	73,425	2,786
−35,0	30,765	1,147	47,646	2,174	75,377	2,817
−17,5	29,408	1,135	48,159	1,881	75,428	2,377
0,0	0,000	0,000	0,000	0,000	0,000	0,000
17,5	27,481	1,249	48,303	1,851	74,576	1,979
35,0	26,640	1,331	49,250	1,823	74,220	2,103
52,5	25,321	1,358	49,533	1,903	72,234	2,337
70,0	24,020	1,894	48,564	2,130	68,045	3,029
87,5	15,733	2,470	34,743	3,043	48,205	3,995

Table 34: Flow Section 3, pressure

Z(mm)	$P_1(m/s)$	$e_1(m/s)$	$P_2(m/s)$	$e_2(m/s)$	$P_3(m/s)$	$e_3(m/s)$
−87,5	21,071	2,012	30,443	3,349	52,871	3,866
−70,0	28,415	1,712	42,366	2,519	69,370	2,711
−52,5	30,156	1,191	45,148	2,500	74,088	2,586
−35,0	30,664	1,078	46,967	2,095	76,409	2,437
−17,5	30,458	1,021	48,932	1,890	77,220	2,409
0,0	−3,044	0,725	−5,798	1,006	−2,791	2,062
17,5	28,141	1,071	49,681	1,785	76,517	1,886
35,0	26,741	1,162	49,746	1,684	74,637	1,978
52,5	25,572	1,250	49,908	1,629	72,273	2,229
70,0	24,581	1,760	49,159	1,936	67,894	2,817
87,5	17,295	2,280	37,596	3,150	50,012	4,028

Table 35: Flow Section 4, pressure

Z(mm)	$P_1(m/s)$	$e_1(m/s)$	$P_2(m/s)$	$e_2(m/s)$	$P_3(m/s)$	$e_3(m/s)$
−87,5	20,183	2,159	29,899	2,797	50,802	3,968
−70,0	28,001	1,828	43,303	2,314	68,144	2,885
−52,5	30,161	1,188	46,008	2,080	72,196	2,538
−35,0	30,956	1,006	48,485	1,944	75,440	2,749
−17,5	30,677	0,929	50,276	1,809	76,229	2,512
0,0	23,560	1,170	39,957	1,753	61,450	2,256
17,5	28,138	1,021	48,843	1,711	76,823	1,748
35,0	27,073	1,077	48,691	1,612	75,309	1,804
52,5	25,451	1,246	48,758	1,557	72,144	2,097
70,0	22,266	2,230	47,791	1,997	67,913	2,822
87,5	15,783	2,282	34,158	2,880	47,932	3,689

Table 36: Flow Section 5, pressure

Z(mm)	$P_1(m/s)$	$e_1(m/s)$	$P_2(m/s)$	$e_2(m/s)$	$P_3(m/s)$	$e_3(m/s)$
−87,5	18,780	2,237	25,526	3,241	47,394	3,931
−70,0	27,578	2,115	37,813	3,577	67,206	3,301
−52,5	29,487	1,657	43,031	2,730	72,179	2,937
−35,0	30,587	1,395	45,834	2,554	74,595	2,904
−17,5	30,350	1,315	48,162	2,204	76,097	2,947
0,0	25,418	1,407	42,369	2,166	65,348	2,589
17,5	28,244	1,338	48,259	2,232	76,582	2,259
35,0	27,054	1,361	48,750	2,105	74,986	2,363
52,5	25,913	1,532	48,668	1,996	72,378	2,644
70,0	23,004	2,307	47,223	2,433	67,102	3,334
87,5	15,570	2,425	34,104	3,169	47,351	4,187

Table 37: Flow Section 6, pressure

Z(mm)	$P_1(m/s)$	$e_1(m/s)$	$P_2(m/s)$	$e_2(m/s)$	$P_3(m/s)$	$e_3(m/s)$
−87,5	17,852	1,977	24,461	2,918	45,636	3,474
−70,0	25,851	2,398	36,340	3,917	64,991	3,382
−52,5	27,698	1,865	42,969	2,728	71,647	2,641
−35,0	29,244	1,441	45,635	2,237	74,796	2,418
−17,5	29,913	0,998	48,055	1,856	74,952	2,691
0,0	25,650	1,022	44,238	1,655	67,701	2,033
17,5	26,773	1,219	47,158	1,839	75,626	1,889
35,0	26,203	1,103	48,419	1,666	74,515	1,858
52,5	24,815	1,351	49,519	1,550	71,370	2,351
70,0	22,692	2,255	47,532	2,140	65,566	2,939
87,5	15,884	2,247	35,179	2,694	44,723	3,526

Table 38: Flow Section 7, pressure

Z(mm)	$P_1(m/s)$	$e_1(m/s)$	$P_2(m/s)$	$e_2(m/s)$	$P_3(m/s)$	$e_3(m/s)$
−87,5	17,784	2,091	26,371	2,904	46,279	3,630
−70,0	23,011	2,810	38,804	3,206	65,404	3,492
−52,5	27,774	1,874	44,418	2,421	73,695	2,388
−35,0	29,678	1,156	47,521	1,994	75,357	2,490
−17,5	29,379	0,807	49,093	1,660	75,281	2,500
0,0	26,150	0,854	45,013	1,415	69,039	1,937
17,5	26,169	0,974	46,350	1,778	74,870	1,800
35,0	26,139	1,078	48,447	1,595	74,747	1,946
52,5	25,762	1,294	48,901	1,519	71,067	2,601
70,0	23,051	1,999	45,695	2,562	62,060	3,932
87,5	17,298	1,953	32,463	2,797	42,908	3,521

A.6.3 *Boundary Layer*

Table 39: Boundary Layer, Section BL1, pressure

$Z'(mm)$	$P_1(m/s)$	$e_1(m/s)$	$P_2(m/s)$	$e_2(m/s)$	$P_3(m/s)$	$e_3(m/s)$
0,0	15,234	0,419	28,103	0,624	52,918	0,664
0,5	17,595	0,448	43,751	0,689	61,584	0,667
1,0	31,424	0,496	55,728	0,651	86,802	0,636
1,5	33,156	0,427	56,228	0,664	87,271	0,768
2,0	33,155	0,596	56,446	0,592	86,527	0,764
2,5	32,718	0,453	56,150	0,633	86,406	0,683
3,0	32,776	0,518	55,701	0,635	86,539	0,680
3,5	32,775	0,605	55,977	0,597	86,380	0,748
15,0	29,364	0,542	52,901	0,612	80,093	0,861

Table 40: Boundary Layer Section BL2, pressure

$Z'(mm)$	$P_1(m/s)$	$e_1(m/s)$	$P_2(m/s)$	$e_2(m/s)$	$P_3(m/s)$	$e_3(m/s)$
0,0	8,896	0,310	18,046	0,488	30,794	0,535
0,5	19,199	0,449	25,029	0,491	45,606	0,568
1,0	25,745	0,383	39,188	0,507	66,278	0,614
1,5	28,287	0,484	46,201	0,497	73,820	0,539
2,0	29,238	0,331	48,522	0,530	76,130	0,572
2,5	29,227	0,401	48,582	0,535	76,382	0,648
3,0	29,083	0,328	48,968	0,457	76,053	0,658
3,5	29,271	0,330	49,321	0,457	75,861	0,585
15,0	27,528	0,516	49,313	0,523	75,046	0,577

A.6.4 *FSI, reinforced*

Table 41: FSI reinforced Section 5, pressure

Z(mm)	$P_2(m/s)$	$e_2(m/s)$	$P_3(m/s)$	$e_3(m/s)$
−87,5	35,135	6,547	64,727	8,876
−70,0	34,649	10,231	57,587	11,248
−52,5	27,100	10,749	29,478	15,149
−35,0	19,011	9,656	6,621	13,750
−17,5	21,856	9,814	12,139	10,422
0,0	38,964	7,374	48,286	10,482
17,5	53,804	6,370	79,402	7,762
35,0	58,348	4,813	87,838	5,028
52,5	60,830	3,471	86,184	4,516
70,0	58,414	3,825	80,526	5,196
87,5	39,487	4,503	56,105	6,026

Table 42: FSI reinforced Section 6, pressure

Z(mm)	$P_2(m/s)$	$e_2(m/s)$	$P_3(m/s)$	$e_3(m/s)$
−87,5	34,786	5,874	54,798	8,560
−70,0	39,116	4,933	57,365	8,396
−52,5	39,774	4,884	53,580	7,319
−35,0	42,191	4,791	53,942	7,276
−17,5	46,686	4,602	61,317	7,514
0,0	50,614	4,475	71,676	7,168
17,5	54,098	4,734	78,869	6,627
35,0	56,093	4,577	81,743	6,104
52,5	57,072	4,099	81,398	5,767
70,0	52,958	4,219	75,737	6,347
87,5	33,899	4,389	51,505	6,215

Table 43: FSI reinforced Section 7, pressure

Z(mm)	$P_2(m/s)$	$e_2(m/s)$	$P_3(m/s)$	$e_3(m/s)$
−87,5	35,371	5,672	54,821	7,146
−70,0	41,052	4,929	59,769	6,370
−52,5	43,328	4,387	61,755	5,954
−35,0	45,760	4,022	64,613	5,971
−17,5	48,963	3,893	69,693	6,186
0,0	51,853	3,977	74,308	6,158
17,5	53,953	4,113	77,882	5,894
35,0	55,436	4,176	79,298	5,602
52,5	54,824	4,213	77,913	5,792
70,0	48,963	4,000	71,215	6,137
87,5	33,863	4,025	51,693	6,052

A.6.5 *FSI, NON reinforced*

Table 44: FSI NON reinforced Section 5, pressure

Z(mm)	$P_2(m/s)$	$e_2(m/s)$	$P_3(m/s)$	$e_3(m/s)$
−87,5	36,881	6,383	68,437	8,661
−70,0	35,637	9,417	62,035	10,396
−52,5	28,995	10,529	37,469	14,177
−35,0	24,954	7,899	20,933	12,366
−17,5	29,672	7,414	18,759	10,623
0,0	42,099	7,830	43,825	13,170
17,5	51,831	6,535	73,395	9,656
35,0	55,782	5,252	83,205	6,740
52,5	59,279	3,207	85,642	4,994
70,0	56,941	3,485	80,220	5,323
87,5	38,862	4,449	56,335	6,055

Table 45: FSI NON reinforced Section 6, pressure

Z(mm)	$P_2(m/s)$	$e_2(m/s)$	$P_3(m/s)$	$e_3(m/s)$
−87,5	34,060	5,731	56,146	7,979
−70,0	39,466	4,683	62,349	7,971
−52,5	42,095	4,418	59,015	7,348
−35,0	43,584	4,263	58,135	6,853
−17,5	47,216	4,501	62,749	7,816
0,0	51,043	4,574	70,118	8,421
17,5	53,947	4,478	76,205	7,294
35,0	55,171	4,422	78,655	6,205
52,5	55,165	4,401	77,575	5,983
70,0	51,868	4,154	72,238	6,303
87,5	34,853	4,368	50,603	6,110

Table 46: FSI NON reinforced Section 7, pressure

Z(mm)	P_2(m/s)	e_2(m/s)	P_3(m/s)	e_3(m/s)
−87,5	36,435	5,214	55,746	6,914
−70,0	42,919	4,395	62,962	6,322
−52,5	44,880	4,091	64,274	5,600
−35,0	46,223	3,773	66,376	5,699
−17,5	49,340	3,731	69,907	6,158
0,0	51,668	3,750	72,876	6,577
17,5	53,935	3,597	74,695	6,258
35,0	55,104	3,587	75,119	5,804
52,5	53,995	3,673	74,045	5,484
70,0	48,044	3,861	65,875	6,088
87,5	34,295	3,893	49,938	5,713

BIBLIOGRAPHY

[1] Fluid structure interaction. URL https://en.wikipedia.org/wiki/Fluid%E2%80%93structure_interaction.

[2] Osas project web page. URL http://osas.no/.

[3] H. Akre, B. Øverland, and O. Skatvedt. Respirasjonsforstyrrelser under søvn. *Tidsskrift for Den norske legeforening Circulation*, 129:1762–1765, 2009.

[4] British Snoring & Sleep Apnoea Association. URL www.britishsnoring.co.uk.

[5] H. F. Becker. Effect of nasal continous positive airway pressure treatment on blood pressure in patients with obstructive sleep apnea,. *Circulation*, 107:68–73, 2003.

[6] B. Broschek and C. Golpe Soñora. Video of flexible plate movement (steady state), 2015. URL http://youtu.be/OLutqWYQc14. Reinforced flexible plate, V3, steady state.

[7] B. Broschek and C. Golpe Soñora. Video of flexible plate movement (transition state), 2015. URL http://youtu.be/DaKJCjIF6p4. Reinforced flexible plate, V3, transitional state.

[8] Yahoo Health. URL http://health.yahoo.com.

[9] A. Van Hirtum, F. Chouly, P.Y. Lagrée, J.R. Paoli, Y. Payan, and X. Pelorson. In r. ferber (ed), when a fluid-structure interaction keeps you awake. *Progress in Sleep Apnea Research, Nova Science Publishers, New York*, pages 41 – 76, 2007.

[10] Singapore General Hospital. URL http://www.singhealth.com.sg.

[11] M. Ip, B. Lam, M. M. T. Ng, W. K. Lam, K. W. T. Tsang, and S. L. Lam. Obstructive sleep apnea is independently associated with insulin resistance. *American Journal of Respiratory and Critical Care Medicine*, 165:670 – 676, 2002.

[12] Habib M'henni, 2010. URL https://commons.wikimedia.org.

[13] G. Mylavarapu, S. Murugappan, M. Mihaescu, M. Kalra, S. Khosla, and E. Gutmark. Validation of computational fluid dynamics methodology used for human upper airway flow simulations. *Journal of Biomechanics*, 42(10):1553–1559, 2009.

[14] NHS. URL http://www.nhs.uk/Conditions/Sleep-apnoea/Pages/Treatment.aspx.

[15] NTNU. Modeling of obstructive sleep apnea by fluid-structure interaction in the upper airways. Description of research project funded by the Research Council of Norway, Internal document, 2014.

[16] Sintef. Mathematics as a means to stop snoring. URL http://www.sintef.no/home/news/sintef-materials-and-chemistry/mathematics-as-a-means-to-stop-snoring/.

[17] F.M. White. *Viscous Fluid Flow*. Mcgraw-Hill Publ.Comp, 1974.